FIXED-PLATFORM BALLISTOCARDIOGRAPHY FOR HEMODYNAMIC MONITORING IN DEEP SPACE

A DISSERTATION
SUBMITTED TO THE DEPARTMENT OF ELECTRICAL ENGINEERING
AND THE COMMITTEE ON GRADUATE STUDIES
OF STANFORD UNIVERSITY
IN PARTIAL FULFILLMENT OF THE REQUIREMENTS
FOR THE DEGREE OF
DOCTOR OF PHILOSOPHY

Corey McCall

June 2022

This dissertation is online at: https://purl.stanford.edu/cz439jk0303

I certify that I have read this dissertation and that, in my opinion, it is fully adequate in scope and quality as a dissertation for the degree of Doctor of Philosophy.

Gregory Kovacs, Primary Adviser

I certify that I have read this dissertation and that, in my opinion, it is fully adequate in scope and quality as a dissertation for the degree of Doctor of Philosophy.

H Heller

I certify that I have read this dissertation and that, in my opinion, it is fully adequate in scope and quality as a dissertation for the degree of Doctor of Philosophy.

Laurent Giovangrandi

Approved for the Stanford University Committee on Graduate Studies.

Stacey F. Bent, Vice Provost for Graduate Education

This signature page was generated electronically upon submission of this dissertation in electronic format. An original signed hard copy of the signature page is on file in University Archives.

Abstract

Spaceflight is known to cause cardiovascular deconditioning and increased risk for cardiovascular diseases due to exposure to microgravity and space radiation. Despite this, astronauts have generally been able to survive spaceflight by monitoring their cardiovascular system and applying countermeasures as needed. However, space agencies have recently shifted their human exploration focus from near-earth to deep space, soon exposing astronauts to longer duration missions aboard smaller proposed "deep space transport" (DST) vehicles. This is unfortunately expected to amplify deconditioning, and the reduced crew volume limits the practicality of most cardiovascular monitoring instruments that have been commonly used on larger space stations where virtually all long duration missions have taken place. Without the ability to practically monitor cardiovascular change in deep space, it is not possible to study its increased effects or efficiently prescribe critical countermeasures.

This work proposes the use of a novel monitoring system designed for DSTs that combines fixed-platform ballistocardiography with other noninvasive sensors to practically measure hemodynamic changes indicative of cardiovascular deconditioning.

The core of the proposed system was a single-dimensional force sensing platform designed to capture the ballistocardiogram (BCG), a measurement of the recoil force of the body in reaction to cardiac ejection. The BCG signal was fused together with signals from a wearable electrocardiogram (ECG) and photoplethysmogram (PPG) to estimate several cardiovascular parameters that can be used to monitor cardiovascular deconditioning. During spaceflight, an astronaut can measure himself or herself with the system by simply maneuvering to the platform mounted to the spacecraft frame, inserting their feet into a coupling, and waiting still for a small number of heartbeats.

The system overcame several engineering challenges in order to accomplish robust signal capture while being operated by a single user in a confined microgravity environment. It also represents the first ever successful use of fixed-platform BCG in microgravity.

To validate the system's quality and practicality, it was first built and characterized, then deployed for human testing in the confined microgravity environment of parabolic flight. In this experiment, the measured BCG signal was compared to the current state-of-the-art alternative, an accelerometry-based BCG designed for free-floating measurement. The proposed system was able to successfully measure standard I and J wave timings of the BCG in all subjects, as well as K wave timings in some of the subjects, while being much less cumbersome than the accelerometry-based BCG system that requires careful manual control of the floating subject. Pulse arrival at the toe and ventricular depolarization timings were also successfully measured in all subjects from the respective PPG and ECG signals. The signal-to-noise ratio of both BCGs were compared, and the BCG measured using the proposed system was higher than the accelerometry-based BCG, suggesting that it is a more robust way to measure BCG in microgravity in terms of signal quality.

After validating the system's quality and practicality, the parabolic flight experiment was expanded to add normal gravity measurements of the same subjects in order to validate that hemodynamic changes could be detected. Comparing the microgravity measurement to normal gravity, significant decrease in RJ interval, increase in pulse transit time, and other changes in hemodynamic parameters were observed. These results were congruent with the expected physiological response, suggesting that the proposed system was able to detect hemodynamic changes induced by microgravity.

With this technology, cardiovascular deconditioning induced by the unique environment of deep space can be more practically studied during upcoming missions, and countermeasures can be more efficiently prescribed using hemodynamic feedback. This represents a step toward safer human deep space travel.

Acknowledgment

None of the work in this dissertation would have been possible without the technical, financial, and emotional support of so many. I am greatly indebted to everyone in this section, and my hope is that our relationship will continue on beyond this PhD in some way.

First, I'd like to thank my advisor, teacher, friend, and the biggest supporter of this work, Professor Gregory Kovacs. Greg is a relentlessly patient person who repeatedly put my well-being and preferences above his own goals. When the quals got the best of me, Greg came through and pulled me out of the rough. When I wanted to clock out for several years to start a company while my research sat on the shelf, Greg remained supportive (and still invited me to the legendary barbecues at his house in Palo Alto). When I struggled to come back and finish, Greg treated every single one of my dozens of failed attempts as if they never happened, and welcomed me back every time with literal open arms. I am thankful that I choose him as my advisor, and it cannot be understated how much his unlimited support enabled me to finally finish this dissertation.

Next, I'd like to thank Laurent Giovangrandi, who also fostered unlimited support for me to complete this work. Laurent is by far the smartest person I have ever met, yet he humbly treats everyone he talks to as an equal colleague. There have been so many times when a 30 minute technical discussion between us (always over espresso) would accelerate my understanding by weeks or months compared to what I would have gathered on my own. In most cases, Laurent has been more of a partner than an co-advisor to me, as he never hesitates to get into the weeds and contribute

alongside student work. He contributed to this work directly by writing the data-capture software used in Section 3.4. I will also never forget the very late nights we spent in Houston and Las Vegas debugging hardware and code hours before a demo or experiment, or soldering together in the 100+ degree airplane hangar between zero-G flights. It has been a great pleasure to work with him.

I'd also like to thank the other members of my dissertation reading and defense committees: Professor Craig Heller (who also flew with us in zero-G!), Professor Bernard Widrow, and Professor Juan Rivas. Your insightful comments and discussions about this work contributed greatly to its final quality.

I'd also like to thank all of the current and former members of the Kovacs group that intersected with my time here: Bill Esposito, Nathan Volman, Zach Stuart, Richard Wiard, Daniel Sohn, Rebecca Rich, Rea Rostosky, Omer Inan, and Allison Korczynski. All of you contributed valuable insight to this work through technical discussions, and most of you were either test subjects in the experiments of Chapters 4 and 5, or assisted in assembling the hardware in Chapter 3. In particular, Richard and Zach contributed significant mechanical design work in Sections 3.5.1 and 3.5.2, and Richard helped with the 3D design of the wearable enclosure in Figure 3.11. Omer contributed electronics designs that were the basis of those used for the BCG and ECG circuits in Section 3.2. Finally, Rea contributed significant logistical and technical writing work with NASA to support the 2014 flight campaign.

I'd also like to thank Marsh Cuttino, NASA's Reduced Gravity Office, NASA Flight Opportunities (Terry Lee, Dominic Del Rosso, and others), and the anonymous test subjects who participated in our experiments. Most of them traveled all the way to Houston for us, and all of them worked hard to make sure our experiments were successful.

This work would have not been possible without the unabated emotional and financial support of my family. My father, Terry McCall, taught me to never give up on on anything, especially my education. My mother, Debbie McCall, has always fought for me and worked with me to make sure that I was able to pursue my dreams inside and outside of school. My sister, Chelsea Kaiser, taught me the value of kindness and the importance of making friends along the way. My grandparents,

Sheryll Hammer, Bob Hammer, and Bonnie Hall, always made sure I had everything I needed to be successful and pursue my goals. Finally, my future wife, Kelly Byron, has been the best partner I could have ever dreamed of (in life and EE labs). I'm not sure she knew all that she was signing up for with our first date after class in 2012, but time has shown that we can happily make it through the best and worst of times as long as we are together.

This work would have also not been possible without the funding from Stanford, Texas Instruments, and the National Science Foundation that supported my studies and the various projects that encompassed my PhD.

Finally, I apologize to anyone I have forgotten to mention here, and ask that you please accept my thanks for all that you have helped me with.

Contents

List of Tables

List of Figures

Chapter 1

Motivation and Applications

Human exploration of deep space is the next major step toward independence from Earth, and promises to unlock countless research opportunities to advance terrestrial technology and our understanding of the universe. Recently, all three of the world's space agencies capable of human spaceflight have aligned toward this same strategic objective with the ultimate goal of a manned mission to Mars and beyond [2–4]. As this new space race commences, one of the most critical unsolved prerequisites for success is ensuring astronaut health while pushing mission distance and duration to unprecedented levels. This dissertation proposes the use of a novel device that partially addresses this prerequisite, specifically for cardiovascular health.

The potential consequences of spaceflight on human physiology have been studied extensively since at least as far back as 1929 [5]. Parameters such as heart rate and blood pressure were even taken on the first manned spaceflight in 1961 in order to study the potential cardiovascular consequences, known as "cardiovascular deconditioning" [6]. Since then, over 550 astronauts have been to Low Earth Orbit (LEO), the space within the inner radius of Earth's radiation-protective Van Allen belts. Through these missions, terrestrial analogs, and animal studies, sufficient countermeasures have been developed such that short missions to LEO, particularly to the International Space Station (ISS), are relatively safe for cardiovascular health and can be conducted on a regular basis [7, 8]. However, deep space travel, beyond LEO, poses unique challenges, and only the 24 astronauts who flew on the Apollo missions

in 1968-1972 have ever experienced its effects. In addition to unique space radiation, deep space missions intrinsically expose astronauts to other environmental factors of spaceflight (e.g., microgravity) for much longer. Currently, less than 10 astronauts have ever experienced a mission longer than 300 days. This extremely limited experience of humans with deep space puts future astronauts at great potential risk for cardiovascular issues. Furthermore, current research suggests that extended deep space travel will likely amplify cardiovascular deconditioning compared to LEO and likely induce or accelerate the development of dangerous cardiovascular disease [1].

Therefore, there is an important need to monitor the cardiovascular system of astronauts on upcoming deep space missions in order to better understand the unique effects of deep space, and create or adapt countermeasures for use aboard the specially designed Deep Space Transport (DST) vehicles that will be used. Currently proposed DSTs also pose an additional challenge in that they are much smaller than the ISS, rendering traditional monitoring systems used on long duration missions cumbersome and impractical. The motivation for this dissertation work was to overcome this challenge and develop technology capable of monitoring cardiovascular deconditioning in a practical way aboard the spatially confined environment of a DST.

1.1 Cardiovascular Dangers of Deep Space

The environment of spaceflight puts unique stressors on the cardiovascular system, ultimately causing cardiovascular deconditioning and related diseases. Some of the effects of these stressors have been studied enough to be well understood, but several gaps and paradoxes still exist. The influence of these environmental stressors on the cardiovascular system are summarized in Section 1.1.1, and the known and potential consequences, and the state-of-the-art in monitoring and countermeasure methods, are introduced in the following sections. These are also discussed again in terms of their specific measurable hemodynamic changes in the context of different types of space environments (i.e., parabolic flight, LEO, deep space) in Section 2.3.

1.1.1 Environmental Influences of Spaceflight

In LEO, the primary environmental change with respect to Earth is reduced gravity ("microgravity"). In deep space, there is also exposure to unique space radiation. Additionally, spaceflight may also expose astronauts to other environmental influences, such as confinement, reduced physical activity, and frequent exposure to pro-oxidative high-oxygen environments such as space suits and vehicles.

Reduced Gravity

Microgravity has two direct and immediate effects on the the cardiovascular system. First, it decreases the hydrostatic pressure gradient along the fluid column of the body according to the equation for vertical pressure variation: $\frac{dP}{dh} = -\rho \cdot g$, where P is pressure, ρ is density, g is gravitational acceleration, and h is height. This eliminates the arterial and venous pressure gradients that normally exists in the direction of gravity, and induces a headward shift of the fluid that is usually pooled in the lower body when upright [9]. This pressure equalization and fluid shift is similar to that of rotating the body from upright to a supine posture in normal gravity. The second effect is the unloading the gravitational force of the surrounding tissue on the cardiovascular system, decompressing all chambers within the body including the thorax, which surrounds the heart and central cardiovascular system [10]. This reduction in intrathoracic pressure reshapes the thoracic cage into a more expanded circular shape, and allows the heart chambers to distend more easily, even compared to a supine posture in normal gravity [10, 11]. In addition to these two immediate changes to fluid position and pressure configurations, microgravity changes the way the body handles movement in two ways that ultimately effect the cardiovascular system: (1) the baroreceptors are no longer exercised during posture change, as the baroreflex is not required to maintain blood pressure during posture changes in the absence of a hydrostatic pressure gradient, and (2) the skeletal muscles require less energy and oxygen since the physical resistance of weightless limbs is much less in microgravity.

Deep Space Radiation

The influence of radiation exposure on the cardiovascular system in deep space is different than on Earth and in LEO, as deep space radiation is unique in both quantity and type. On Earth, humans are subject to an average dose of about 3 millisieverts (mSv) per year of radiation [12], or about 6 mSv in countries with pervasive medical imaging such as the United States [13]. During its transit to Mars in 2011 and 2012, the Curiosity rover measured an average expected exposure to astronauts of about 1.8 mSv *per day* [14]. The Curiosity measurements, combined with research studying radiation induced cancer risk to astronauts [15], estimate the expected exposure on a round trip mission to Mars to be between 0.5-1.0 Sv. Additionally, deep space radiation is uniquely composed of protons and heavy high-energy ("HZE") ionic particles, also known as high linear energy transfer particles, that are not blocked by the Van Allen belts as they are on Earth. These types of particles are generally more dangerous than terrestrial x-rays or gamma rays in terms of biological damage [16], and are much more difficult to shield since they are more penetrating and interact with shielding in a way that cannot be mitigated by increasing shield density [17].

Research on how specifically deep space radiation affects the cardiovascular system is extremely limited, as only the Apollo astronauts have ever been exposed to it. However, radiation damage to the cardiovascular system after exposure to terrestrial radiation has been studied in the context of radiotherapy and nuclear incidents, and has been shown to cause particular dysfunction and inflammation of the vascular endothelium, which is critical to cardiovascular function and part of many cardiovascular disease pathologies [18, 19].

1.1.2 Deconditioning and Spaceflight-induced Cardiovascular Disease

The environmental influences in Section 1.1.1 generally result in maladaptations, or "deconditioning," of the cardiovascular system and an increased risk for cardiovascular disease. The major effects of these maladaptations and a brief explanation of their associated pathophysiology are presented in this section and summarized in Figure 1.1

below. These major effects are: reduced baroreflex effectiveness, accelerated arterial stiffening, reduced cardiorespiratory fitness, and increased risk for ischemic heart disease and other vascular diseases. More detailed reviews of these effects can be found in [1, 20].

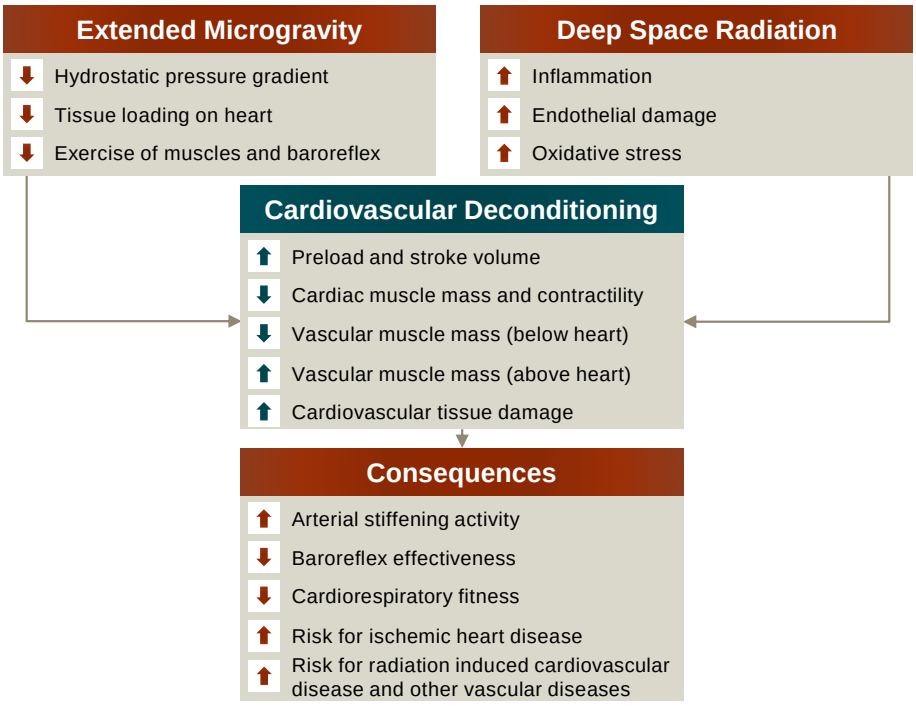

Figure 1.1: Summary of the cardiovascular dangers of deep space and their consequences.

Reduced Baroreflex Effectiveness (Orthostatic Intolerance)

Orthostatic intolerance is the inability to maintain adequate upper body and cerebral blood pressure during orthostatic stress, sometimes resulting in syncope in an upright position, but not in a reclined position. This condition has been widely reported to occur in astronauts post-spaceflight with an incident rate of about 20% for short-duration flights (4-18 days), and about 80% for longer-duration flights (129-190 days) [21]. It poses a health risk not only in post-spaceflight recovery, but also because astronauts need to maintain mobility and cognitive abilities during their

gravity-dependent descent to Earth, during landing in case of emergency, and during extravehicular activity (EVA) in non-zero gravity environments such as on the Moon or Mars.

Spaceflight-induced orthostatic intolerance can be generally considered a reduction in baroreflex effectiveness. The baroreflex is a negative feedback mechanism that senses blood pressure deviation from an adaptive operating point via stretch-sensitive mechanoreceptors called baroreceptors located in the atria, aortic arch, and carotid sinuses, and mediates an immediate (within a few cardiac cycles) counter response via the autonomic nervous system (ANS). Decreased distention of the vasculature near the baroreceptor activates the sympathetic branch of the ANS, resulting in increased blood pressure by increasing cardiac output by means of increased heart rate and contractility, as well as increased vasoconstriction by means of vascular smooth muscle contraction. Increased distention of the vasculature lowers sympathetic activity and activates the parasympathetic branch of the ANS, which has a functionally opposite effect on the same systems to lower blood pressure, decreasing both cardiac output and vasoconstriction.

For reasons that are not completely understood, astronauts who experience post-spaceflight orthostatic intolerance are unable to fully activate these ANS-controlled compensatory mechanisms despite decreased distention in their upper vasculature when hydrostatic pressure is reintroduced. This is likely related to respective hormonal- and neural-mediated compensatory hypovolemia [22] and vasodilation [23] in response to the increased preload and stroke volume that occur due to the microgravity-induced fluid shift mentioned in Section 1.1.1. However, orthostatic intolerance has been reported immediately after flight, even after volume loading countermeasures were used [21]. Controlled studies using lower body negative pressure (LBNP) in-flight to slowly introduce hydrostatic pressure have shown that the baroreflex is successfully able maintain adequate pressure at very low LBNP (between –15 and –30 mmHg) [24], but at higher magnitude LBNP (–50 mmHg), the ability to induce vasoconstriction rapidly reduces while the heart rate response remains intact, albeit inadequate to maintain blood pressure [25]. This indicates that perhaps the microgravity operating

point of the baroreflex with respect to vasoconstriction adapts to be close to its maximum, leaving very little reserve capacity to compensate for orthostatic stress. This is consistent with the well-known paradox that although the increased preload and stroke volume of microgravity induce compensatory vasodilation, sympathetic activity remains uncharacteristically elevated compared to a ground-based reference [26]. This unexplained nature of baroreflex malfunction highlights the need for the cardiovascular system to be further studied in spaceflight, particularly as mission durations increase to unprecedented lengths.

Accelerated Arterial Stiffening

Arterial stiffening is a normal part of the biological aging process that slowly degrades the central elastic arteries by means of deteriorating the function and quantity of elastin in the arterial wall, and decreasing arterial caliber through the natural buildup of plaque ("atherosclerosis"). Through several mechanisms outlined below, increased arterial stiffness can ultimately lead to cardiac failure and major organ damage. Notably, it has been reported that after six months of spaceflight in LEO, some astronauts have experienced stiffening of the carotid artery equivalent of more than 20 years of aging [27]. An example of this thickening is shown in Figure 1.2, adapted from [1], below. Other studies have shown stiffening or thickening of the aortic [28] and femoral [29] arterial walls as well. This is a health risk when returning back to earth where the astronaut will to continue to age, and also to astronauts with preexisting elevated stiffness that may be more quickly increased to life threatening levels during the mission, especially if they plan to remain in an extraterrestrial environment, such as a planetary base, for an extended time.

When the central arteries are healthy, they have capacitive elastic walls that allow them to buffer the intermittent "pulse waves" of pressure from the left ventricle, smoothing them out and lowering their velocity and amplitude before they enter the periphery, and providing kinetic energy for flow during the diastolic period between pulses. Elasticity also creates the compliant side of a protective "stiffness gradient" that increases from the ejection site to the organs, allowing high energy waves to be partially reflected before entering peripheral circulation [30]. Arterial stiffness

attenuates this buffering effect [31], and reduces the stiffness gradient between the central and peripheral arteries, inducing high systolic pressure (maximum pressure) and pulse pressure (range of pressure) in the periphery that can cause organ damage, particularly to low-impedance high-flow organs such as the the brain and kidneys [30, 32,33]. Additionally, increased pulse wave velocity (PWV) causes the wave reflections from the stiffness gradient and arterial terminations to arrive back at the heart too quickly while the heart is still early in systole, increasing the workload on the heart and further increasing systolic pressure [34]. This increased workload on the heart has been shown to cause maladaptive left ventricular hypertrophy and remodeling, which can lead to heart failure [35].

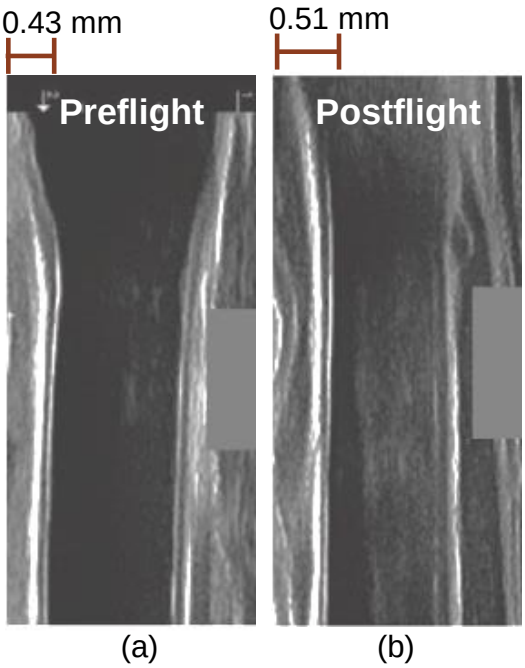

Figure 1.2: Ultrasound image (adapted from [1]) of the common carotid artery measured proximal to the carotid bulb in an astronaut (a) preflight, and (b) after 6 months of spaceflight. The difference in wall thickness is equivalent to more than 20 years of normal aging.

In space, arterial stiffening can occur through several verified mechanisms, and has the potential to increase through mechanisms anticipated in deep space. Stiffness from wall-thickening of arteries higher in the body (above the heart) have been observed in spaceflight [27], as is the expected adaptation of the walls to increased distending pressures compared to an upright posture in normal gravity [36]. Similar stiffening has also been observed in arteries lower in the body that are not subject to increased distending pressures [28,29], and is thus a result of other adaptations to environmental influences of spaceflight. For example, the headward fluid shift triggers a sustained increase in renin–angiotensin–aldosterone system activity [37], which is expected to stiffen arteries through endothelial dysfunction and stimulation of collagen formation, matrix remodeling and hypertrophy, and proliferation of vascular smooth muscle cells [38]. Other environmental influences of spaceflight such as increased sympathetic activity [24], increased oxidative stress from increased exposure to pro-oxidative environments [39], reduced physical activity [40], and confinement [41] can all also contribute to arterial stiffening through similar mechanisms. Space radiation is also expected to directly increase oxidative stress through ionization, and likely cause endothelial dysfunction [19], potentially increasing arterial stiffening further. No data has been published on direct measurements of endothelial dysfunction in spaceflight on the Apollo missions or otherwise, and it has been highlighted as an urgent area for future research [1]. These arterial stiffening acceleration mechanisms of spaceflight, and the potential for increase due to deep space radiation, further highlight the need for the cardiovascular system to be further studied in spaceflight during longer and farther missions.

Reduced Cardiorespiratory Fitness

Reduced cardiorespiratory fitness is defined as a reduction in maximal oxygen consumption (VO_2 max), the maximal aerobic capacity of the astronaut [42]. It has been observed on long duration missions, particularly when not counteracted with exercise [43]. It results in reduced physical performance, and is likely the cause of excessive fatigue and tachycardia that has been observed during stressful mission tasks such as EVAs [44]. Prolonged periods of zero gravity have also been shown to reduce

tolerance for physical exertion [43]. It is important that astronauts in deep space are able to maintain high physical performance considering that EVAs and strenuous exploratory or emergency tasks are likely to be required.

Cardiorespiratory fitness reduction and its imposition on physical performance happens when cardiac and skeletal muscle mass is reduced, both of which have been observed in astronauts. Skeletal muscle atrophy is likely due to to the fact that the range of motion of astronauts is different in microgravity compared to Earth, and current exercise countermeasure prescriptions do not employ high enough resistance and contractions over ranges of motion that would normally be unnecessary on Earth to preserve normal muscle mass [45]. Cardiac muscle atrophy has also been directly observed in space and in ground-based microgravity analogs, and may be due to reduced blood volume loading on the heart compared to a supine position [46]. Computational models have also shown a reduction in myocardial contractility, the heart's innate ability to contract, versus ground-based supine models due to spaceflight-induced deconditioning [47]. The potential for reduced cardiorespiratory fitness due to insufficient countermeasures and potential changes to the heart muscle highlight the need to measure trends in VO_2 max during space missions in order to optimize countermeasures.

Increased Risk for Ischemic Heart Disease and Other Vascular Diseases

Ischemic Heart Disease (IHD) is the leading cause of premature mortality [48]. It occurs when bloodflow to the heart muscle is restricted or stopped due to atherosclerosis in the heart's arteries. This leads to oxygen starvation and scarring of the heart's muscle cells, potentially resulting in deadly heart attacks or arrhythmias. In addition to IHD, atherosclerosis is also associated with increased risk of stroke and other cardiovascular and cerebrovascular diseases [49].

On Earth, exposure of the heart to high levels of ionizing radiation is known to be associated with IHD in the context of radiotherapy [50], and exposure to ionizing radiation is expected to increase dramatically in deep space as discussed in Section 1.1.1. HZE radiation has also been tested on human cells and in mice, and has been shown

to accelerate atherosclerosis [51], inhibit angiogenesis [52], and promote an inflammatory response in heart tissue [53], all of which increase risk for cardiovascular diseases. Long term studies of the Apollo astronauts who were exposed to deep space radiation have also been done, in which cardiovascular disease mortality was higher than a similar cohort of astronauts only exposed to LEO, astronauts who have never been to space, and the same age group in the United States population [54]. However, these results have been challenged due to the small sample size of astronauts, the lack of matching the cohorts based on other cardiovascular risk indicators, and other reasons [55]. Additionally, just as in the previous section on accelerated arterial stiffening, the adaptation of cardiac preload, stroke volume and left atrial size to the weightlessness induced fluid shift will accelerate arteriosclerosis, potentially further increasing the risk of IHD [20]. The increased risk for IHD and other vascular diseases that will likely affect astronauts in deep space again further highlights the need for the cardiovascular system to be further studied in deep space.

1.1.3 Countermeasures and Active Monitoring

In order to counteract cardiovascular deconditioning, astronauts employ a strategy of monitoring their cardiovascular system and applying countermeasures. Classical cardiovascular monitoring devices used in LEO in modern spacecraft and the ISS are described below along with typical countermeasures. In the next section, Section 1.1.4, a more recent cardiovascular monitor based on ballistocardiography is presented as the most similar technology to the solution described in this dissertation.

Countermeasures

A portion of cardiovascular deconditioning can be counteracted, most commonly with aerobic and restive exercise. For example, an astronaut can strap themselves to a treadmill with bungee cords, strap into an indoor cycle, or use a rowing machine or resistance bands. However, there is still much work to be done in this field. First of all, exercise does not restore hydrostatic pressure gradients, so many of the deconditioning effects due to headward fluid shift are still uninhibited. For example,

exercise has been shown to be insufficient in preventing some vascular changes such as arterial stiffening and intima-media thickness increase, even during medium-duration missions [27, 29]. The effect of exercise compared to no exercise has also never been studied, as no long duration spaceflight has ever been conducted without exercise, questioning the effectiveness of exercise as a countermeasure [56].

As periodic exercise remains the state of the art countermeasure for cardiovascular deconditioning, research continues into other methods to counteract the effects of the headward fluid shift in particular. Most of these research efforts are focused on artificial gravity in the form of centrifugation and LBNP. Centrifugation studies with and without concurrent exercise have shown that VO_2 max loss and orthostatic intolerance can be counteracted by intermittent use of a centrifuge [57–59]. In the case of orthostatic intolerance, this is done by overcoming the lack of dynamic sympathetic response mentioned in Section 1.1.2 [60]. LBNP is much simpler to employ than a centrifuge, especially with concurrent exercise, and has been shown to be similarly effective in bed rest analog studies [61]. In addition to these, fluid volume loading can reduce orthostatic intolerance temporarily in critical situations (e.g., during a landing) [62].

The only reliable countermeasure for radiation is shielding, but shielding is much more difficult in deep space [16]. This is because deep space radiation is more energetic, containing HZEs, which subjects shielding materials to nuclear fragmentation, in which the high energy radiation particles shatter the shielding particles into smaller showers of ions that cannot be counteracted by higher density material like terrestrial radiation can. Instead, lighter, hydrated materials are being developed to better counteract the effect of nuclear fragmentation since electromagnetic energy loss and nuclear fragmentation per unit mass have been found to increase with decreasing atomic number of the target [63].

Most of these countermeasures, especially exercise, are costly in a mission-oriented environment where any time spent doing countermeasures is valuable time taken away from scientific activities. This highlights the importance of better gauging cardiovascular deconditioning levels so that countermeasures are not over or under

prescribed. This could possibly be achieved with a practical monitor such as the one described in this dissertation.

Active Monitoring

Many of the classic gold standard noninvasive cardiovascular monitoring instruments can work work in LEO, although most are not compatible or practical for deep space. These instruments track up to four key parameters potentially indicative of cardiovascular deconditioning: cardiac contractility, cardiac output, arterial stiffness, and blood pressure. For example, a transthoracic echocardiogram (TTE), a noninvasive ultrasound of the heart, is capable of measuring cardiac output and contractility, but requires a technical expert to give the exam and interpret the results, as well as a cumbersome procedure. It also cannot measure other key parameters such as arterial stiffness and blood pressure without being combined with other instruments. In LEO, a TTE exam can be given remotely by an operator guiding the astronaut from Earth in real time using relatively low latency data communication [64]. However, in deep space, the operator would need to be onboard to administer the complex exam since this type of communication would not be possible due to the high data latency associated with longer distances. A brachial sphygmomanometer could be used to monitor changes in blood pressure, and with the addition of a tonometer or other device for determining pulse transit time (PTT), it could also estimate arterial stiffness [65]. However, to measure the other key parameters, the device would require additional equipment for contractility and cardiac output such as a TTE or large inert gas rebreathing system. Overall, these device configurations would not be practical in deep space because of their multi-instrument complexity, cumbersomeness, or requirement for low latency communication with an expert.

Two device configurations that would be able to measure the four target parameters are a continuous noninvasive arterial pressure (CNAP) device, or a combination of an impedance cardiogram (ICG), a measurement of the impedance across the heart measured from four skin electrodes, and distally placed photoplethysmogram (PPG), an optical measurement of the relative local fluid volume beneath the skin. In the latter case, the PPG could be replaced by a tonometer or any other technology for

gathering distal pulse timing. The first device, a CNAP, typically utilizes a "vascular unloading" technique in which a pneumatic pump is used in a control loop with a PPG in order to precisely apply pressure to a finger cuff such that the measured volume in the finger remains constant. The pressure cuff signal in this case is equal to the arterial pressure. Waveform analysis on this signal can yield the other key metrics [66, 67]. However, CNAP devices require a complex setup that takes a long time to complete and attach to the subject, making it very cumbersome.

The other device configuration that can measure all four key parameters is an ICG combined with PPG, where the ICG is able to measure contractility and cardiac output, and the PTT calculated between the ICG and PPG pulse can be used to track changes in arterial stiffness and blood pressure [65]. This configuration is a less cumbersome solution than CNAP, but still suffers from the fact that ICG requires four sticky electrodes to be precisely placed on the subject under their flight suit, which may be difficult for a non-expert.

Overall, there exists an opportunity to develop a technology that is more practical and less cumbersome at monitoring changes in the four target parameters.

1.1.4 Recent Technologies for Hemodynamic Monitoring in Microgravity

In addition to the more standard monitoring mentioned in the previous section, researchers have also proposed effective, less traditional monitoring modalities. For example, the Astroskin™(Carre Technologies, Inc., Montreal) smart garment contains an ECG, respiration sensor, pulse oximeter, skin temperature sensor, activity-recognizing accelerometer, and a PTT-based blood pressure monitor embedded into the surface of a special wearable shirt and hat. It was co-developed and tested in space with NASA and the Canadian Space Agency [68], and is proven to be less cumbersome than traditional instruments considering that it employs ambulatory monitoring while the astronaut is doing other activities. It is indeed less cumbersome, but is unable to measure changes in the target parameters such as cardiac output and contractility.

The current state of the art related to the research in this dissertation is a method

called accelerometry-based ballistocardiogram (BCG), in which a small accelerometer is fixed close to the astronaut's center of mass (typically their lower back) as they free-float in microgravity [69,70]. The BCG is a measurement of the body's recoil reaction to the ejection of blood by the heart with each heartbeat [71], and is discussed at length in the following chapter. Using this BCG technique, combined with a device to measure distal pulse timing such as a PPG, enables monitoring of changes to all four target parameters as validated on various types of BCG sensing devices: Cardiac Output [72], Contractility [73], Arterial Stiffness [65] and Blood Pressure [65,74,75], all within an easily wearable form factor. However, the major drawback of accelerometry-based BCG is its requirement of uninterrupted free-float over the course of many heartbeats in order to take a measurement. Free-floating on a small spacecraft is extremely difficult without being interrupted because of the high probability of colliding with a wall, equipment, or other astronauts. For example, in a study aboard a space-confined parabolic flight, researchers on the forefront of this technology could only use 5.6% of the data recorded because of issues with uninterrupted free-float [76]. This was despite the fact that they had a crew of "operators" attempting to avoid collisions between the subject and objects. This unfortunately restricts its use on small vehicles such as DSTs.

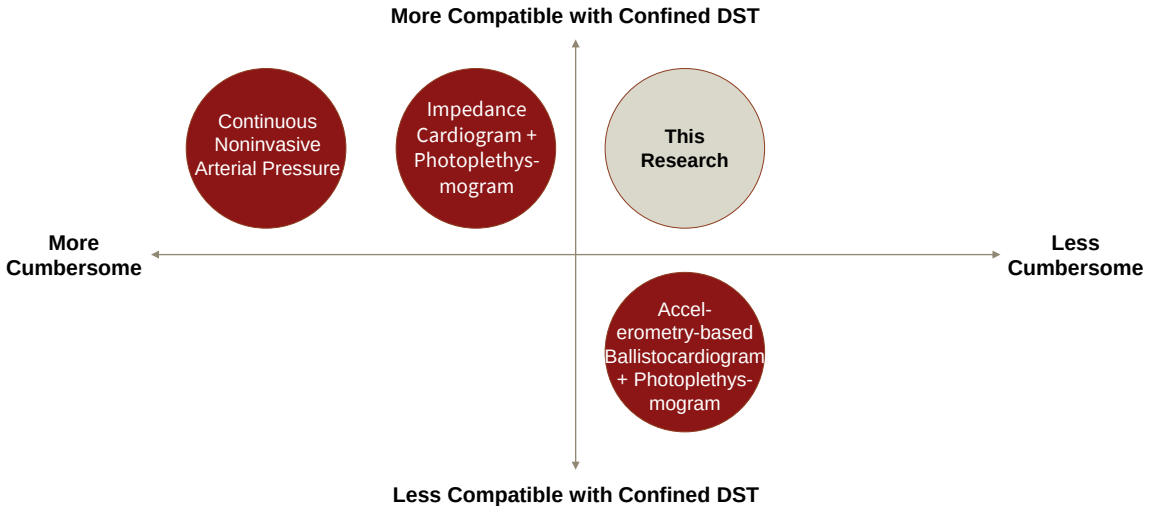

Figure 1.3: Summary of the research in this dissertation compared to other devices capable of measuring the target parameters.

Therefore, there is a research opportunity for a practical monitoring device that can perform at least as well as accelerometry-based BCG in the confined environment of DSTs, while maintaining the ability to measure the four target parameters. Figure 1.3 above summarizes the comparison between the research in this dissertation and other devices capable of measuring the target parameters.

1.2 Fixed-platform Ballistocardiography for Hemodynamic Monitoring in Deep Space

To address this research opportunity, we employ a technology called "fixed-platform BCG," which is similar to state of the art accelerometry-based BCG, but less cumbersome, particularly in the confined environment of a DST, in that it does not require unimpeded free-floating. It has also been subject to more clinical validation in terms of measuring the target parameters [72–74, 77]. Instead of measuring acceleration of the body due to cardiac ejection recoil, fixed-platform BCG measures the downward force that the recoil transfers to the lower body via a strain gauge mounted between the foot of the user and a fixed wall or floor. This technology is discussed at length in the next chapter, and represents the first time this type of BCG has been adapted to and tested in microgravity.

In order to realize this unique application of fixed-platform BCG, and demonstrate its superiority compared to the current accelerometry-based BCG state of the art, the engineering objectives of this dissertation were set as follows:

1. To devise methods for enabling robust measurement of BCG across a population of subjects in the similarly confined microgravity environment of parabolic flight

2. To quantify the quality of the signals obtained with respect to the alternative state of the art free-floating BCG

3. To validate that a number of features in the BCG combined with ECG and PPG are able to detect cardiovascular parameter changes relevant to cardiovascular deconditioning

With these objectives met, the designed system would be validated as a method for acquiring clinically valid BCG signals in a confined microgravity environment. The major next step, which is not within the scope of this dissertation, would be to test its sensitivity to actual spaceflight-induced cardiovascular change in the environment of a space transport vehicle or analog.

Chapter 2

Ballistocardiography for Deep Space

Ballistocardiography was chosen as a core technology because of its ability to measure the four target parameters, and the ability of its platform form factor to function conveniently in a very confined area. From its discovery in late 19th century [78], the field of ballostocardiography has recently experienced a revival in research beginning in the early 2010's [79]. This new research, particularly on the clinical validation of the platform-based BCG (or scale-based BCG as it is referred to in most previous literature) [72, 73] and on the genesis of particular features of the signal [80], has enabled a robust and convenient clinical device that could be adapted to deep space in this dissertation. This chapter describes the BCG's history, theory, and functionality, as well as its target application to deep space missions. The remaining chapters of this dissertation focus on the design, implementation, and clinical validation of a novel microgravity-compatible BCG device for use in deep space.

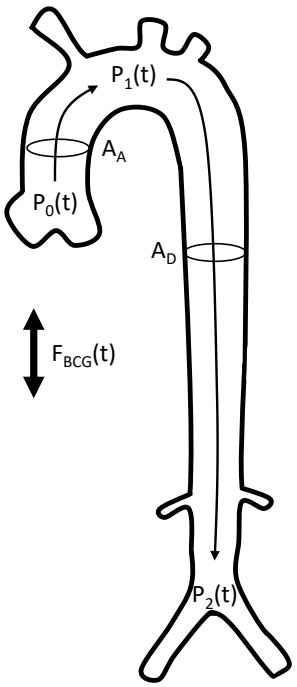

Figure 2.1: Sketch of the aorta showing cross-sectional areas and blood pressure measurement locations in Equation 2.1. The long arrows indicate the direction of flow from ejection.

2.1 BCG-based Hemodynamic Measurement

The BCG is a measurement of the body's recoil reaction to the ejection of blood by the heart with each heartbeat. As a hemodynamic instrument, it contains information primarily about blood pressure gradients created in the aorta by the ejection as modeled in [80]:

$$F_{BCG}(t) \approx A_D[P_1(t) - P_2(t)] - A_A[P_0(t) - P_1(t)] \tag{2.1}$$

where F_{BCG} is the time-dependent BCG signal, which is a force, A_D and A_A are the average cross-sectional areas of the descending and ascending aorta respectively, modeled as connected tubes. P_0, P_1, and P_2 are the the blood pressure at the inlet

of the ascending aorta, apex of the aortic arch, and outlet of the descending aorta respectively. These labels are shown in Figure 2.1 above. Although the $P_1 - P_2$ and $P_0 - P_1$ gradients (which change the velocity of the blood mass within the tube) are the primary drivers of the BCG signal, it is also noted that the volume flow rates at the inlet and outlet of the aorta (which change the blood mass within the tube) also contribute to the recoil force. However, the impact of the flow rates were found to be mathematically insignificant in magnitude compared to the pressure gradients [80].

In order to measure the BCG, the body should ideally be isolated entirely within the instrument's measurement mechanism, where the whole-body force, acceleration, or velocity can be measured and filtered to the expected bandwidth of the BCG features of interest. This bandwidth is usually 0.1–10 Hz for platform-based measurements where the subject stands still on a floor-mounted sensor such as in this dissertation [81]. However, low-pass filtering is usually designed with cutoff frequencies of at least 25 Hz when measured along with higher bandwidth signals (e.g., ECG) in order to preserve the accuracy of inter-signal time intervals [82]. Notably, this low bandwidth frequency range is susceptible to special noise conditions when the sensor is mounted to the floor, such as floor vibrations from nearby walking, and the subtle movement of a person trying to stand still on the platform. These can be dealt with using either adaptive filtering or gating, which has been shown to be successful in [83] and [84] respectively.

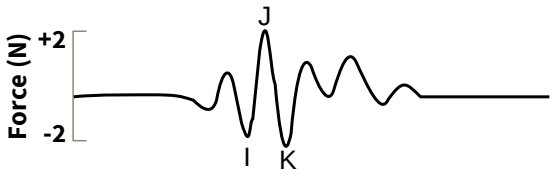

Figure 2.2: BCG waveform of a single heartbeat recorded using a platform-based BCG device. I, J, and K indicate the most commonly analyzed waves within the BCG signal.

The BCG is usually interpreted by the timing and amplitude of three points on its major waveform: the I wave, J wave, and K wave, as labeled in Figure 2.2 above. According to the model in Equation 2.1, the I wave peaks when $P_0(t) - P_1(t)$ is

maximal. This is when $P_0(t)$ is in systole, and $P_1(t)$ is still in diastole. The force direction reverses when $P_1(t)$ enters systole while $P_2(t)$ is still in diastole, and peaks at the J wave when this maximizes $P_1(t) - P_2(t)$. The force direction then reverses again as $P_2(t)$ enters systole, reducing $P_1(t) - P_2(t)$ to its minimum at the peak of the K wave.

According to this analysis of the pressure gradients and the model in [80], it can be gleaned that the timing of the initial part of the I wave may be thought of as the base of the pulse wave entering the ascending aorta, and the peak of the J wave may be thought of as the base of the pulse wave exiting the descending aorta. The ability to calculate this base-to-base aortic PTT is very valuable, in that aortic PTT is a well known predictor of cardiovascular risk, particularly if the length of the aorta is known in order to calculate PWV [85]. Furthermore, the amplitude of the J wave can be thought of as the aortic pulse pressure (the difference between the systolic and diastolic pressure) scaled by A_D, which may be used to indicate relative changes to aortic pulse pressure, which is correlated to relative changes in stroke volume [86].

The major limitation to this direct analysis of the BCG waveform is that the core study [80] validated Equation 2.1 by comparing outputs of the model (derived from invasive blood pressure measurements) to the expected shape and timing of the BCG waveform instead of validating it against actual BCG waveforms from the test subjects. However, many other studies have been done comparing BCG waveforms to clinical parameters such as the target parameters in this dissertation as described in the sections below:

2.1.1 Contractility

Changes to myocardial contractility can be observed by measuring changes in the preejection period (PEP), the time interval between the beginning of electrical depolarization (Q wave of the ECG) and the first outflow of blood from the left ventricle (e.g., the B wave of an ICG) [87]. It was observed in [73] that previous research [88]

estimating PEP changes using an ECG and a mechanocardiogram, a back-worn instrument that measures valve-related vibrations, could be modified to use a fixed-platform BCG, which measures flow-related vibrations. It was subsequently found that the BCG yielded a similar result to the mechanocardiogram. The RJ interval, the time between peak electrical depolarization (R wave of the ECG) and the peak of the BCG's J wave, was correlated with with the PEP ($R^2 = 0.86$ across 10 subjects and 2,162 heartbeats while modulating the PEP using the Valsalva maneuver) [73]. Thus, it was also correlated with contractility. Similarly correlated results were also achieved in other research using a head-mounted BCG and ECG [89]. In this way, the BCG, combined with an ECG, can be used to measure changes in contractility via changes in the RJ interval.

2.1.2 Cardiac Output

Cardiac output is the product of stroke volume and heart rate. Stroke volume is the more difficult measurement, as heart rate can be measured by simply counting the heart beats per time period in a BCG, ECG, or PPG signal. As mentioned in Section 2.1, stroke volume is likely correlated with the amplitude of the BCG J wave, as the J wave amplitude scales with pulse pressure which is correlated with stroke volume. This was tested in [72], where the percentage change in the root-mean-square (RMS) power of the BCG was found to be correlated with changes in cardiac output as measured by Doppler echocardiography ($R^2 = 0.85$ across 9 subjects and 275 heartbeats while modulating the cardiac output with exercise recovery). Considering that the J wave contains most of the power in the BCG signal, this also aligns with the model in Equation 2.1. Therefore, BCG can be used to measure changes in stroke volume and cardiac output via changes in the RMS power of the BCG signal.

The formula for calculating the moving RMS power of the BCG signal and its percent change are given in Equation 2.2 and Equation 2.3 respectively from [72]:

$$BCG_{rms}[k] = \sqrt{\frac{1}{A}\sum_{i=0}^{A-1} BCG[k+i]^2} \qquad k = 1, \ldots, N_{sample} - A \tag{2.2}$$

$$\Delta BCG(\%)[k] = (\frac{BCG_{rms}[k] - BCG_{rms,rest}}{BCG_{rms,rest}}) \times 100\% \tag{2.3}$$

where A is the width of the sliding window in samples, $BCG_{rms}[k]$ is the moving RMS power calculated at sample k, and $BCG_{rms,rest}$ is the baseline RMS power.

2.1.3 Arterial Stiffening

Changes in arterial stiffness can be measured via PWV changes within the aorta. It can also be measured as changes in PWV between a proximal and distal point that includes the aorta, although this is a less accurate method because of the existence of smooth muscle in the peripheral vessels that effect PWV. Arterial stiffness and PWV are related by the Moens-Korteweg formula [90]:

$$PWV = \sqrt{\frac{E_{inc} \cdot h}{2 \cdot r \cdot \rho}} \tag{2.4}$$

where E_{inc} is the incremental elastic modulus, and the constants h, r, and ρ are the vessel wall thickness, radius, and density of blood respectively. The challenge of measuring PWV is in choosing a proximal and distal measurement point that is convenient and includes the aorta. The clinically popular carotid-femoral measurement can be taken by measuring the pulse timing at each site using a tonometer [91]. Another popular method is called pulse arrival time (PAT), which is the time between the ECG R wave peak and a distally measured PPG pulse (e.g., finger or toe) [92]. This method is convenient because in many scenarios, particularly ambulatory applications, an ECG is easier to obtain than using tonometry, and it is difficult to acquire a proximal pulse with a PPG. However, the PAT method has been repeatedly criticized in literature because of its inclusion of the PEP in addition to the PTT, which is modulated independently of arterial stiffness [93, 94]. Fortunately, fixed-platform BCG provides an excellent proximal pulse marker at the I wave, the beginning of the pulse wave entering the ascending aorta [80]. In fact, it may even be possible to simply use the timing between the I wave and the J wave to calculate PTT as in [95], since the J wave peak may indicate the base of the pulse exiting the descending aorta

as discussed in Section 2.1. However, this method is still early on in research. In this dissertation, PTT, and thus a correlate to PWV and arterial stiffness, was measured between the I wave of the fixed-platform BCG and a toe-mounted PPG.

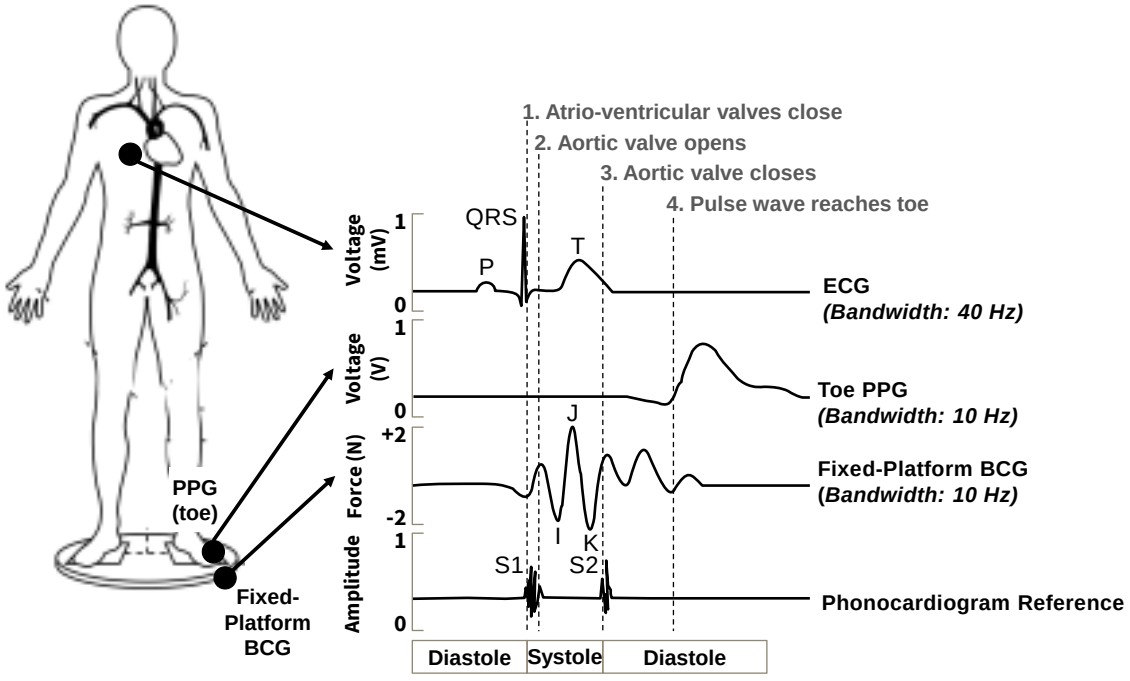

Figure 2.3: Example of the three main signals recorded by the instrument developed in this dissertation: ECG, toe PPG, and fixed-platform BCG. For orientation, a phonocardiogram reference is also shown along with markers for major events within the cardiac cycle.

2.1.4 Blood Pressure

PWV can also be used to estimate blood pressure, as the Bramwell-Hill equation relates the PWV of an incompressible fluid in an elastic tube to the pressure within the tube in [90]:

$$PWV = \sqrt{\frac{A \cdot dP}{\rho \cdot dA}} \tag{2.5}$$

where P is blood pressure, ρ is blood density, and A is the tube's cross-sectional area. Outside of this theoretical model, blood pressure correlation studies have also been done on fixed-platform BCG, in which it was found that the BCG RJ interval is also moderately correlated with systolic ($R^2 = 0.59$ across 10 subjects while modulating the blood pressure using the Valsalva maneuver) and diastolic ($R^2 = 0.30$ in the same experiment) pressures when compared to a CNAP device [74]. However, it was later found that this correlation does not hold for faster pressure changes induced by paced respiration like they do for the slower time scale Valsalva [75]. Therefore, although blood pressure changes were not calculated directly in this dissertation, it is recommended that future work use PWV rather than RJ interval based methods for blood pressure calculation.

2.1.5 Combining BCG With Other Hemodynamic Sensors

In this dissertation, in order to maintain compatibility with the four target parameters, the fixed-platform BCG system was combined with both an ECG and PPG as shown in Figure 2.3 above. This expanded the fixed-platform BCG's capabilities as an instrument as discussed in the previous sections of this chapter, and also allowed for cross-signal denoising methods such as ensemble averaging which is discussed more in Section 3.6.2.

2.2 Volume Limit Comparisons

The volume aboard DSTs is expected to be extremely limited, which is what makes accelerometry-based BCG so difficult to conduct without detrimental noise artifacts from collisions. One way to quantify this is by looking at the pressurized volume of the different potential vehicles. Note that pressurized volume is not equivalent to habitable volume since equipment and storage is often within the pressurized compartment. However, pressurized volume is a standard specification that is easy to compare. Table 2.1 below shows the pressurized volume for four different vehicles: the Orion capsule being designed for short-duration deep-space travel (e.g., moon

missions) [96], the NASA Deep Space Habitat being designed for 500-day deep space missions [97], the current ISS [98], and a standard Boeing 727-200 passenger cabin [99]. The Deep Space Habitat is less than half the pressurized volume of the ISS where almost all long duration missions have taken place thus far. The habitable volume is even less considering that up to 500 days of supplies must also be stored onboard compared to the ISS which can be easily resupplied. The Orion capsule has a pressurized volume almost 10x smaller than the Deep Space Habitat.

Table 2.1: Pressurized Volume of Different Vehicles

Vehicle	**Pressurized Volume (m^3)**
Orion Capsule	20
NASA Deep Space Habitat (500 day configuration)	193
ISS	425
Boeing 727-200 Cabin	186

The instrument developed in this dissertation is designed to function in as little space as possible. Although it could not be tested in the exact configuration of the Orion capsule or NASA Deep Space Habitat (which have yet to be finalized), it was able to be tested in the same microgravity environment that the current state of the art, accelerometry-based BCG, was tested in– the Boeing 727-200 cabin. In these tests, which are described in detail in Chapter 4 and Chapter 5, the platform-based BCG device was fixed to the surface of the cabin, as it would be in any vehicle, and the experiments were conducted using approximately 15% of the cabin volume, as the remainder was reserved for other researchers, equipment, and permanent seating.

2.3 Expected Hemodynamic Changes of Cardiovascular Deconditioning

Cardiovascular deconditioning, as described in Section 1.1, negatively affects the cardiovascular system over time as astronauts are exposed to microgravity and other deep space environmental factors. For a hemodynamic monitor to be successful, it should be able to monitor as many of the hemodynamic changes associated with

these changes as possible. These changes are described in Sections 2.3.1–2.3.3 as they progress from very short-term parabolic flight microgravity to long-term flight in deep space. The specifics of how the instrument developed in this dissertation measures them is discussed in Section 2.3.4.

2.3.1 Parabolic Flight

In interplanetary space, astronauts are subject to true microgravity in the absence of major gravitational fields. Microgravity is also achievable in the environment of a free-falling vehicle such as an orbiting spacecraft in LEO, or during parabolic flight. In these cases, the vehicle itself maintains a free fall permanently during an orbital trajectory, or temporarily during the upper segment of a parabolic trajectory. The free-fall, combined with the cabin's shielding from aerodynamic resistance, creates an inertial frame of reference that enables microgravity.

On parabolic flight, passengers experience multiple approximately 17-second microgravity segments separated by normal and "hypergravity" segments during the plane's recovery. So long as care is taken to not disturb the hemodynamic system during the hypergravity segments (i.e., lying down instead of sitting or standing to reduce downward fluid shift and compensatory responses), these short microgravity segments begin with a fast, smooth transition from normal gravity in the supine position. Since these segments are so short, there is not time for any cardiovascular remodeling or hemodynamic operating point changes, thus only transient reactions are expected.

Echocardiography studies have shown that the left atrium distends immediately by 3.6 mm after the transition to microgravity compared to the normal gravity supine position [10, 100]. At the same time, the transmural central venous pressure (TCVP) increases by 4.3 mmHg, increasing preload [10]. This is likely because of the expansion of the thoracic cage due to the gravity unloading of the surrounding tissue, as confirmed by a decrease in esophageal pressure of 5.6 mmHg. Cardiac output has also been confirmed to increase compared to the normal gravity supine position, indicating an increase in venous return [101].

2.3.2 Low Earth Orbit and Longer Duration Spaceflight

After the transient effects of microgravity, the body's hemodynamic systems begin to adapt to sustained microgravity. For example, during the first day of flight, about 2 liters of fluid from the legs slowly shift to the upper body and stabilizes at this level for the duration of the flight [102]. This results in a large increase in pressure in the upper veins, as exemplified by a 5 to 21 mmHg increase in the left internal jugular vein measured after 50 days of flight [103]. TCVP remains elevated compared to the normal gravity supine position for the same reasons stated in Section 2.3.1 [20], maintaining increased cardiac output and stroke volume due to the Frank-Starling mechanism. This increase in cardiac output and stroke volume is even greater when measured later in flight after several months, although the reason for this is currently unknown [20]. Blood pressure measured with CNAP [104] and at the brachial artery [105] both show a decrease compared to the normal gravity supine position, even more so on longer flights [20]. Systemic vascular resistance decreases [23], despite an increase in sympathetic nerve activity as discussed in Section 1.1.2 [26]. Heart rate generally does not change, and there has not been any evidence of arrhythmia developing up to 6 months into flight [20]. Finally, although it has not been measured directly, computational models show a likely reduction in myocardial contractility after 5 months of flight [47].

2.3.3 Deep Space

With respect to the hemodynamic systems of the body, the principle difference between long duration LEO flights and deep space is exposure to deep space radiation. The primary concern is whether this radiation will induce structural damage to the cardiovascular system, via inflammation of the vascular endothelium as discussed in Section 1.1.1, or otherwise. The field of deep space radiation-induced cardiovascular diseases remains extremely limited, and has mainly been studied in mice models where it was shown that deep space equivalent radiation combined with weightlessness (simulated via hindlimb unloading) did indeed induce endothelial damage in a way that is known to lead to occlusive artery diseases [106]. Further human research

in this field is required, again highlighting the need for a practical hemodynamic monitor for deep space such as the one in this dissertation.

2.3.4 Mapping Cardiovascular Deconditioning to Target Parameters

The fixed-platform BCG + ECG + PPG system described in Figure 2.3 on page 25 is able to measure trends in most of the hemodynamic changes described in Sections 2.3.1–2.3.3, with the exception of upper body venous pressure. Changes in preload from altered TCVP can be tracked using the RJ interval, as it is inversely correlated with the preejection period. Myocardial contractility can also be tracked via changed in the RJ interval as discussed in Section 2.1.1. Changes in cardiac output can be tracked via changes in the percentage change in RMS power of the BCG as discussed in Section 2.1.2. Changes in blood pressure can be tracked via PWV analysis as discussed in Section 2.1.4. Finally, changes in systemic vascular resistance can be tracked by comparing cardiac output with blood pressure changes (e.g., increased cardiac output at the same time as decreased or unchanged blood pressure indicates a decrease in systemic vascular resistance). Therefore, the device developed in this dissertation is able to adequately monitor the expected hemodynamic changes during spaceflight, and thus potentially cardiovascular deconditioning itself.

Chapter 3

Instrument Design

The design of the instrument discussed in this dissertation was guided by a set of system requirements described in Section 3.1. These requirements included both core requirements for the instrument itself, as well as research requirements to validate its functionality. The electrical designs of the instrument are discussed in Sections 3.2–3.4, the mechanical design of the instrument is discussed in Section 3.5, and the software postprocessing of the collected signals is discussed in Section 3.6. The limitations of the design and suggested future work are discussed in Section 3.7, and finally, the design of the instrument as a whole is summarized in Section 3.8.

3.1 System Requirements

In order to accomplish the engineering objectives of this dissertation stated in Section 1.2, the following core requirements were adopted for the device:

C.1. **Fixed-platform BCG:** The fixed-platform BCG was required to be functional without gravity in a small space, where functional was defined as able to detect at least the I wave and J wave features for a diverse population while attached to a powered vehicle.

C.2. **PPG:** The PPG was required to be easily adjustable to different skin tones and toe sizes in order to detect the pulse arrival timing for a diverse population.

In addition to the core requirements, the following research requirements were also adopted. These were not necessary to deploy a working device, but were required to test and validate the instrument in the following chapters, and were thus part of the design:

R.1. **Data Capture:** A reliable real-time data capture and monitoring system was required in order to monitor experiments for issues (e.g., subjects moving too much, or sensor reading anomalies).

R.2. **Hardware Durability:** Physical hardware was required to resist vibratory interference from the vehicle, and survive incidental impacts from the researchers and objects.

R.3. **ECG:** Reliable detection of R waves was required.

R.4. **Accelerometry-based BCG:** An accelerometry-based BCG was required to replicate the current state of the art for comparison.

R.5. **Accelerometer:** An accelerometer was required to mark the microgravity sections in the collected dataset.

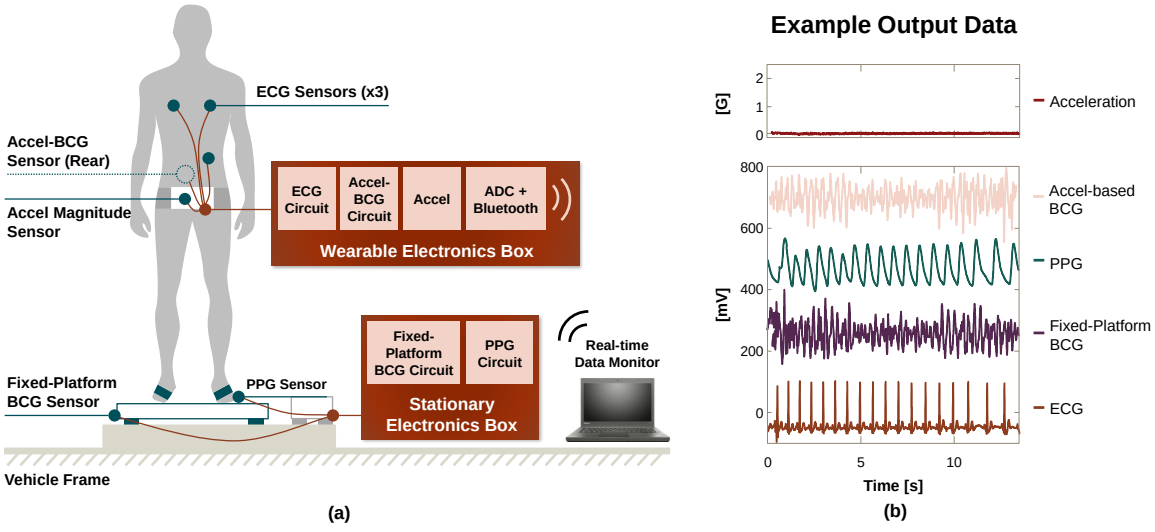

Figure 3.1: (a) System-level diagram of the complete instrument and validation setup, showing each sensor's placement. (b) Example waveforms from the system.

Figure 3.1 above shows a diagram of the design and where each sensor was placed according to these two groups of requirements, as well as an example of the data captured.

3.2 Electrical Design: Standard BCG and ECG Amplifiers

In order to accomplish requirements C.1, R.3, and R.4, circuits similar to those in [81] were employed for fixed-platform BCG, ECG, and accelerometry-based BCG respectively. These are described in Sections 3.2.1–3.2.4, and in Figure 3.2 below.

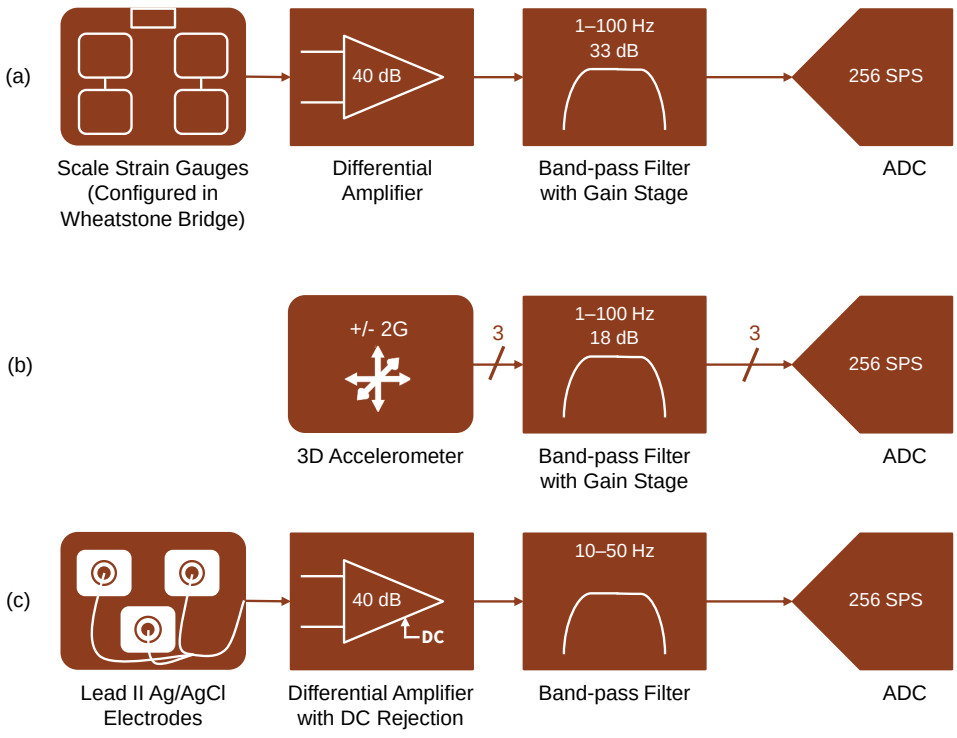

Figure 3.2: Block diagram of standard circuits employed for (a) fixed-platform BCG, (b) accelerometry-based BCG, and (c) ECG.

3.2.1 Fixed-platform BCG Amplifier

The fixed-platform BCG sensor was an InnerScan® BC-534 weighing scale (Tanita®, Tokyo, Japan), which was previously fully characterized for BCG capture in terms of linearity and frequency response in [81]. The strain gauge of the scale was configured in a Wheatstone bridge and connected to an AD8226 instrumentation amplifier (Analog Devices®, Wilmington, MA) with a gain of 40 dB. The output was then amplified 33 dB by a non-inverting gain stage using an LT1885 operational amplifier (Linear Technology®, Milpitas, CA), then band-pass filtered to 1–100 Hz by a passive high-pass filter and 4th-order Sallen-and-Key low-pass filter. The final stage of the signal chain was connected to an analog-to-digital converter (ADC), sampling at 256 Hz. A block-diagram representation of this circuit is given in Figure 3.2(a) above.

3.2.2 Free-floating Accelerometry-based BCG Amplifier

The accelerometry-based BCG sensor was an LIS344ALH micro-electromechanical system accelerometer (STMicroelectronics®, Switzerland) with a range of +/− 2 G, sensitivity of 0.67 mV/mG, and noise density of 50 µG/$\sqrt{\text{Hz}}$. The individial analog outputs of each axis were connected to separate identical non-inverting gain stages and band-pass filters with similar makeup and characteristics to the fixed-platform BCG circuit (18 dB, 1–100 Hz). The stages were AC-coupled in this design to remove any imperfections in the microgravity segments of parabolic flight. The final stage of each signal chain was then connected to a different channel of the same ADC as the fixed-platform BCG. A block-diagram representation of this circuit is given in Figure 3.2(b) above.

3.2.3 ECG Amplifier

The ECG sensors consisted of three 3M-2570 Ag/AgCl gel electrodes (3M®, Saint Paul, MN) placed on the chest and stomach near the left arm, right arm, and left leg in a Lead II configuration. The right arm and left leg electrodes were wired to the respective negative and positive inputs of an AD8226 instrumentation amplifier with a gain of 40 dB, and the left arm electrode was connected in a right leg drive

configuration. The reference input of the instrumentation amplifier was configured for DC rejection. The signal was then band-pass filtered to 10–50 Hz by a passive high-pass filter and 4th order Sallen-and-Key low-pass filter in the same way as the fixed-platform BCG circuit. The final stage of the signal chain was connected to a different channel of the same ADC as the BCGs. A block-diagram representation of this circuit is given in Figure 3.2(c) on page 33.

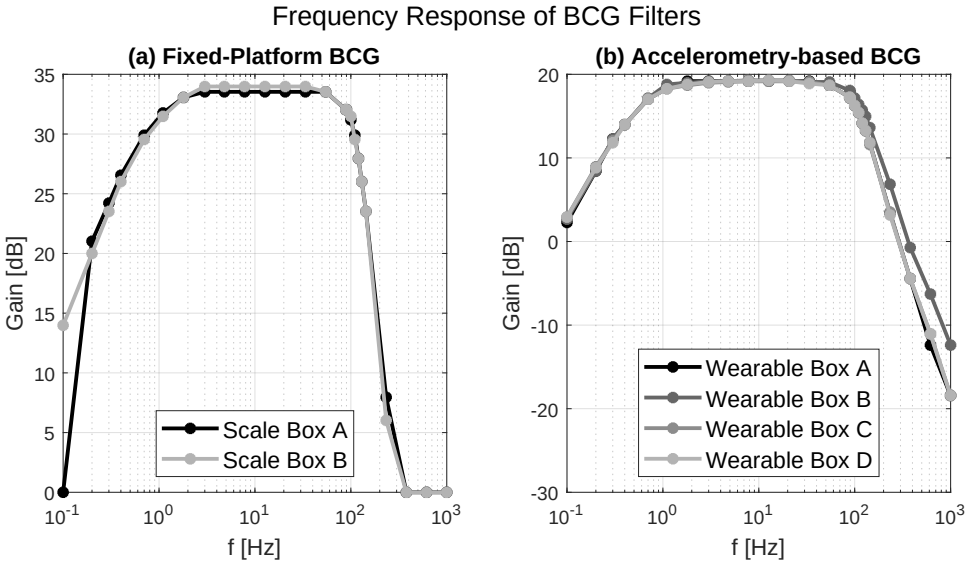

Figure 3.3: Measured frequency response of (a) fixed-platform BCG, and (b) longitudinal accelerometry-based BCG filter stages. Each trace represents a specific instance of the hardware.

3.2.4 BCG Calibration

In order to accommodate multiple subjects, two fixed-platform and four accelerometry-based BCG circuits were built. The gain and bandwidth of the final stage filters on these circuits were measured in order to verify the bandwidth, and calibrate the output to force and acceleration units respectively for each device. These measurements are shown in Figure 3.3 above. The average mid-band gains of the fixed-platform BCG circuits were 32.9 dB and 33.1 dB for "Scale Box A" and "B" respectively, and the average mid-band gains of the accelerometry-based BCG circuits were 18.5 dB,

18.8 dB, 18.4 dB, and 18.4 dB for "Wearable Box A", "B","C", and "D" respectively. In addition to the final stage filter gain, the fixed-platform BCG circuit also had a 47 dB differential gain from the input instrumentation amplifier stage which is in addition to the filter gain.

In order to convert the fixed-platform BCG ADC counts (12 bits) to Newtons for an individual circuit, the following calculation was made using the force to differential voltage across the Wheatstone bridge of $19.1\mu V N^{-1}$ given in [81] that used the same scale:

$$\begin{aligned} BCG[N] &= (BCG[counts] - \frac{2^{12} counts}{2}) \cdot \frac{3V}{2^{12} counts} \cdot \frac{10^6 \mu V}{1V} \cdot \frac{1N}{19.1\mu V} \cdot \frac{1}{gain} \\ &= \frac{1}{gain}(38.35 \cdot BCG[counts] - 78,534) \end{aligned} \tag{3.1}$$

In order to convert the accelerometry-based BCG ADC counts to Gs, the following calculation was made using the accelerometer output range of $3V = +/-2G$:

$$\begin{aligned} Accel[G] &= (Accel[counts] - \frac{2^{12} counts}{2}) \cdot \frac{3V}{2^{12} counts} \cdot \frac{4G}{3V} \cdot \frac{1}{gain} \\ &= \frac{1}{gain}(9.77 \cdot 10^{-4} \cdot Accel[counts] - 2.00) \end{aligned} \tag{3.2}$$

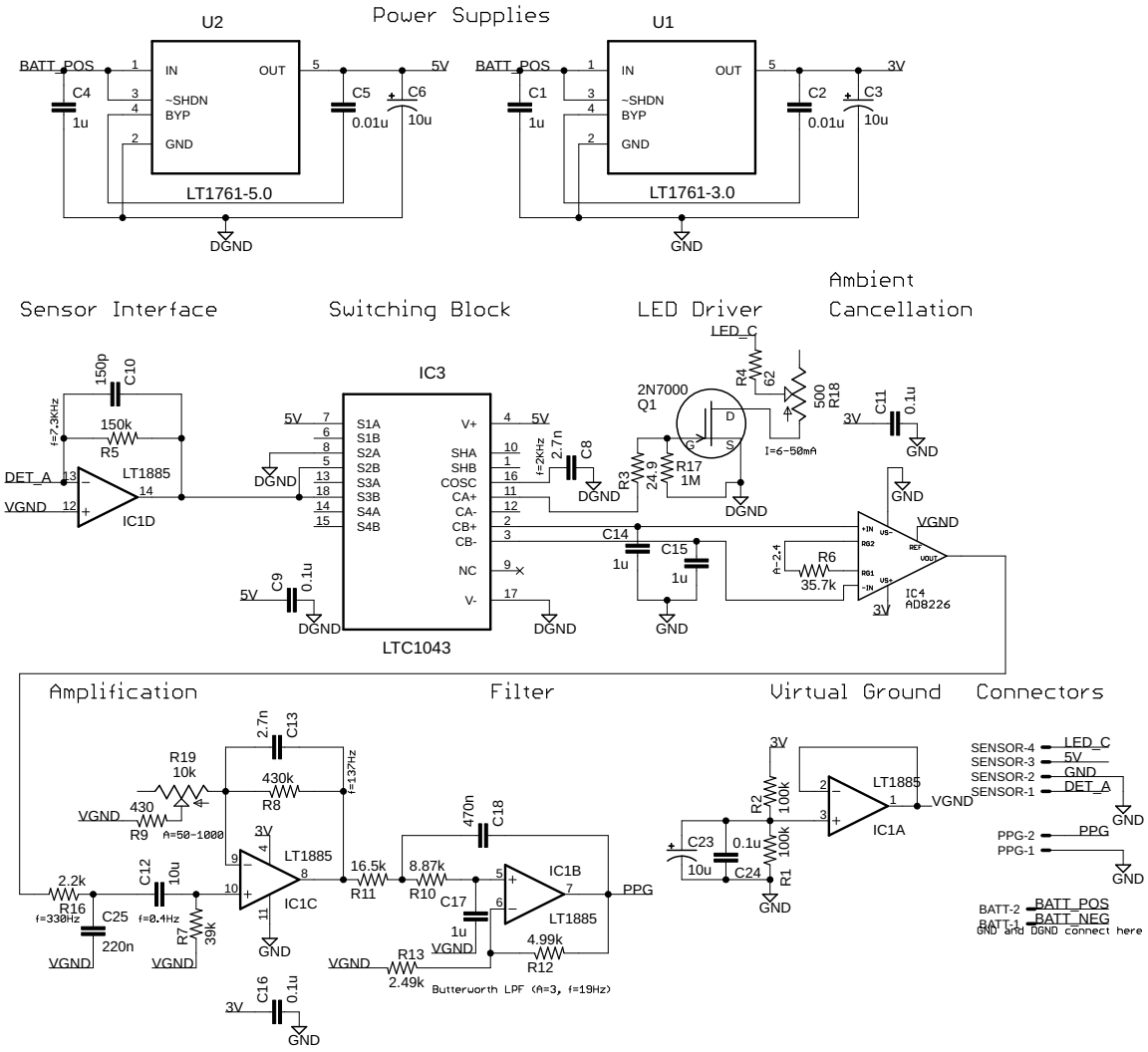

Figure 3.4: Full circuit schematic for custom adjustable PPG design.

3.3 Electrical Design: Adjustable Toe-PPG Amplifier

In order to accomplish requirement C.2, a custom adjustable gain circuit was designed to measure the PPG from the toe. With this type of adjustability, the gain of the sensor as well as the excitation LED could be easily adjusted to suit different skin types using potentiometer knobs. The circuit design and schematic are described in Section 3.3.1.

3.3.1 Design and Schematic

The circuit consisted of $5V$ and $3V$ power supplies, and 8 sections, as shown in Figure 3.4 above. The first section, Sensor Interface, was a transimpedance amplifier that converts the current from an 8000J PPG photodiode sensor (Nonin Medical Inc., Plymouth, MN) to a voltage. The second section, Switching Block, employed a Linear Technology LTC1043 switched capacitor building block configured in such a way to gate the output of the first section at 2 KHz into two segments depending on if the Nonin 8000J excitation LED was on or off. This allowed later stages of the circuit to differentiate between ambient light sensed by the Nonin 8000J and ambient + excited light. The third section, LED Driver, was a simple transistor-based driver for the Nonin 8000J LED with an adjustable current limiting resistor, R18. This resistor limited the current between 6 and 30 mA depending on the position of the potentiometer knob. Section 4, Ambient Cancellation, was an Analog Devices AD8226 differential amplifier with an input of C14 and C15 sample and hold capacitors. These capacitors held the value of the ambient and ambient + excited photodiode readings between gating, allowing for the output signal of this stage to subtract the ambient light readings from the ambient + excited light to reduce noise from ambient light changes. Section 5, Amplification, was a 0.4 Hz passive high-pass filter and an active non-inverting gain stage adjustable from 43-70 dB via potentiometer R19. Section 6, Filter, was the final stage in this signal chain in which the output was second-order low-pass filtered to 19 Hz with an additional gain of 9.5 dB. Section

7, Virtual Ground, was an active reference to mid-supply, and Section 8, Connectors, hosted external connectors to the Nonin 8000j, output, and battery.

3.4 Electrical Design: Shimmer® Data Logging and Accelerometer

The final electrical requirements, R.1 and R.5 were accomplished using a commercial off-the-shelf Shimmer® 2R module (Shimmer Research®, Dublin, Ireland). The Shimmer® 2R featured wireless real-time data logging of a multi-channel ADC, as well as an internal accelerometer sensor. Custom MATLAB® (Mathworks®, Natick, MA) software was developed to monitor and record the data collection in-flight on a nearby laptop. Figure 3.5 below shows a screenshot of this software as well as a photo of the Shimmer® module.

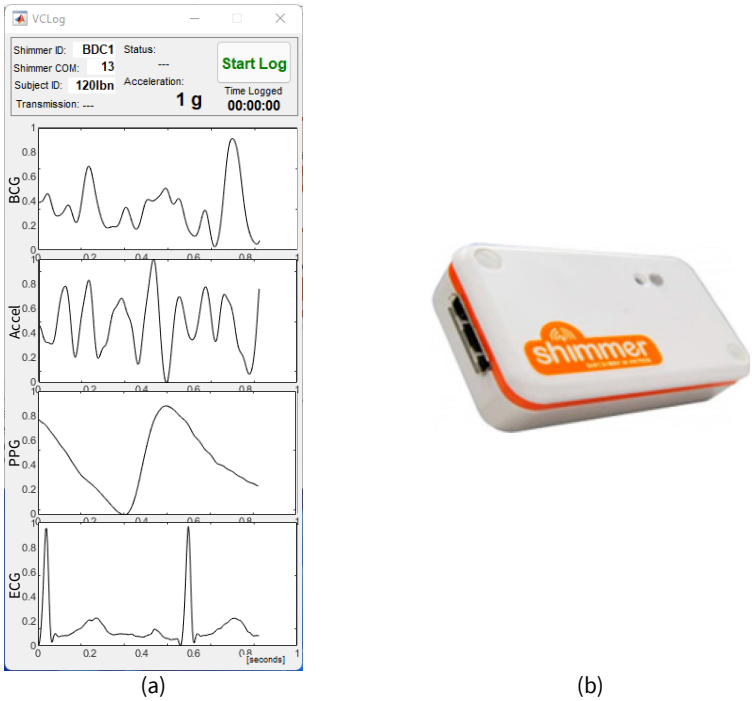

Figure 3.5: (a) Screenshot of custom MATLAB® real-time data logging software, and (b) photo of Shimmer® 2R module used to transmit the data to the logging software.

3.5 Mechanical Design

The final requirement, R.2, called for the final assembly to be robust against foreign object collisions, and resilient to vibrations from the vehicle. The mechanical coupling and vibration isolation of the instrument to the vehicle is discussed in Section 3.5.1. The way the subject was attached to the instrument in microgravity is discussed in Section 3.5.2. The way the sensors and electronics were attached to the instrument and subject are discussed in Section 3.5.3. Finally, the characterization of the assembled mechanical system is discussed in Section 3.5.4.

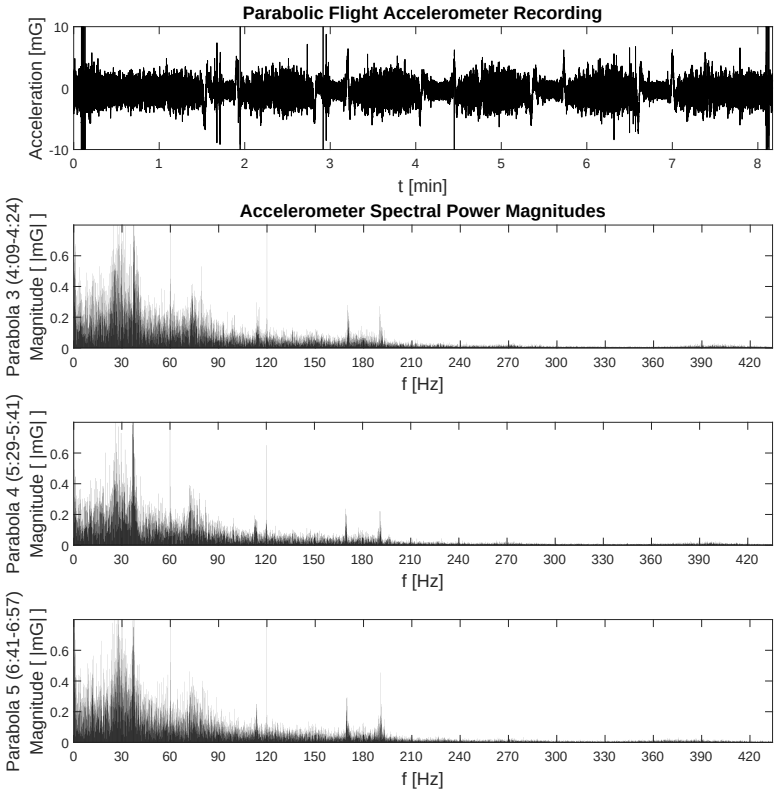

Figure 3.6: Parabolic flight accelerometer recording (row 1), and the spectral power magnitudes of three example parabolas (rows 2–4).

3.5.1 Mechanical Coupling of BCG Platform to Vehicle

Before the experiments took place, a single-axis accelerometer was flown aboard the parabolic flight aircraft, mounted to the floor, in order to measure the vibration the plane produced in the direction of the fixed-platform BCG sensor. Figure 3.6 above shows an example of these measured vibrations, indicating significant noise concentration in the low-frequency range where BCG is measured (1–10 Hz).

In order to improve this, the scale sensor was attached to a mounting plate that was mounted to the vehicle using four vibration isolating assemblies, shown in Figure 3.7 below. Each of these assemblies contained four Sorbothane® (Sorbothane®Inc., Kent, OH) viscoelastic isolator disks, sandwiched between two washers and a locking washer to secure the isolator to the vehicle mounting thread. The Sorbothane® material was sized to maximally isolate vibrations at 30 Hz, adequately above the BCG bandwidth as discussed in Section 2.1. AN-6 studs were then threaded into the vehicle mounting thread and secured with a jam nut. The isolator assembly was then compressed 10%–20% in length using the wing nut, and the wing nut was secured in place using liquid thread locker.

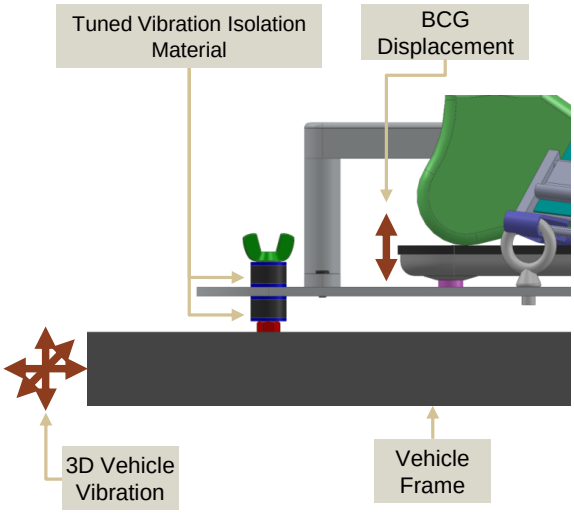

Figure 3.7: Side view model of the scale sensor attached to the vehicle via one of four vibration isolating assemblies.

3.5.2 Securing Subjects to the BCG in Microgravity

In order to attach subjects to the fixed-platform BCG sensor, Lexa® snowboard-style foot bindings (Burton®, Burlington, Vermont) were attached to the assembly via a baseplate as shown in Figure 3.8 below. The foot bindings provided strong coupling between the subject and the assembly, and also a quick release mechanism to easily release the subject if evacuation were required. In this assembly, the foot bindings were attached to a baseplate that was mounted to the main mounting plate with a crossbar and rubber stanchion. During the assembly procedure, the crossbar and stanchion compressed the scale with pressure in order to secure it in place and preload the scale's strain gauge. This was necessary since the DC bodyweight component does not exist in microgravity, so without preload, the scale sensor would only function in a single direction (compression).

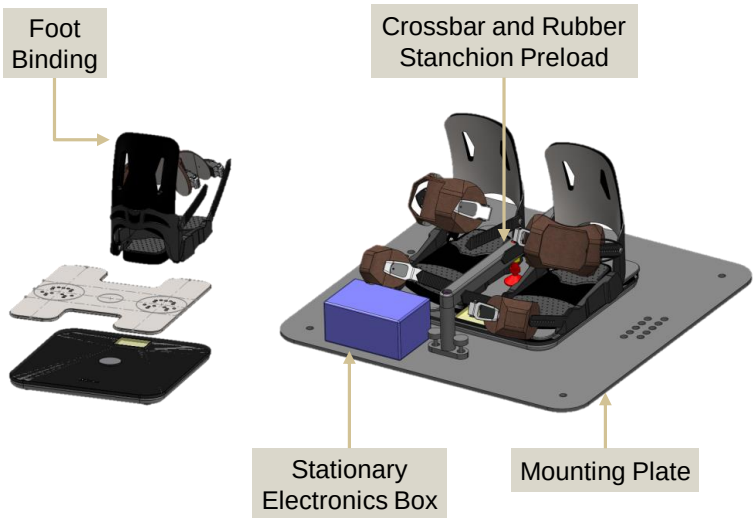

Figure 3.8: Snowboard-style foot bindings were attached to a baseplate (left) which was mounted with the scale to the main mounting plate using a crossbar and stanchion (right).

In order to protect both the subjects and equipment during potential microgravity collisions, protective foam and hole-punched tennis balls were attached to most edges and posts of the assembly as shown in Figure 3.9 below.

Figure 3.9: Photo of subject latched into instrument. Protective foam and tennis balls protected the equipment and subjects during microgravity collisions.

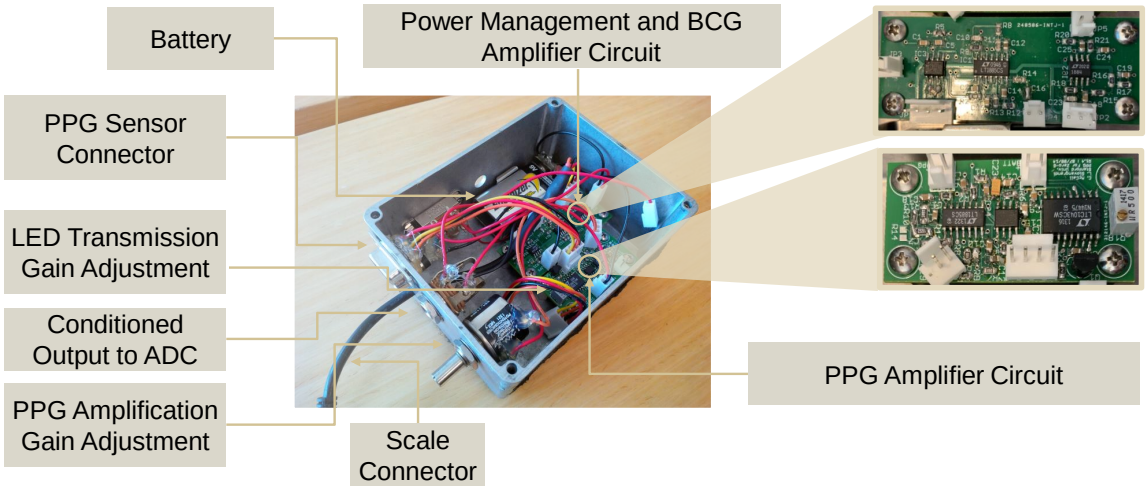

Figure 3.10: Enclosure mounted to the main mounting plate housed the power management and fixed-platform BCG amplifier circuit, PPG amplifier circuit, and external connectors including the PPG gain adjustment knob.

3.5.3 Sensor and Electronics Enclosures

In order to mount the electronics to the instrument and protect them from potential collisions, two enclosures were designed. The first is shown in Figure 3.10 above, which housed the power management and fixed-platform BCG amplifier circuit, the PPG amplifier circuit, and external connectors including the PPG gain adjustment knob. This metal box was grounded, providing electronic shielding, and attached to the main mounting plate with Velcro® (Velcro® IP Holdings LLC, Manchester, NH). When a new subject used the instrument, they connected a cable from their toe-mounted Nonin 8000J PPG sensor to the enclosure where indicated in Figure 3.10 above.

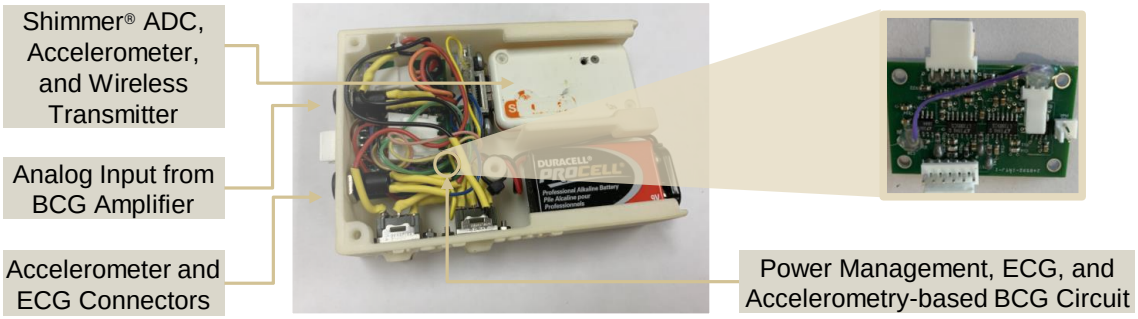

Figure 3.11: Wearable enclosure housed the ECG and accelerometry-based BCG amplifier circuits, and the Shimmer® module.

The second electronics enclosure is shown in Figure 3.11 above, and housed the ECG and accelerometry-based BCG amplifier circuits, and the Shimmer® module. This enclosure was strapped to the waist of each subject. The accelerometry-based BCG sensor was then attached to the subject's lower back with medical tape, and the ECG electrodes were attached in a Lead II configuration using 3M-2570 gel electrodes. Finally, a two-conductor shielded cable was connected to the other enclosure in order for the Shimmer® module to receive the fixed-platform BCG and PPG signals.

With the assembly isolated from vehicle vibrations and all parts protected from collisions, requirement R.2 was now met, finally fulfilling all requirements in Section 3.1.

3.5.4 Characterization of the Crossbar-mounted System

The assembled mechanical system was characterized via the Fourier transform of its impulse response. This was done to test how different crossbar preloadings affected the system's gain and delay as measured by the strain gauge. This was important because the amount of crossbar preloading was not standardized during experiments, and some subjects were measured without the crossbar while on the ground in normal gravity. The error induced by this varying of crossbar preloadings is determined below.

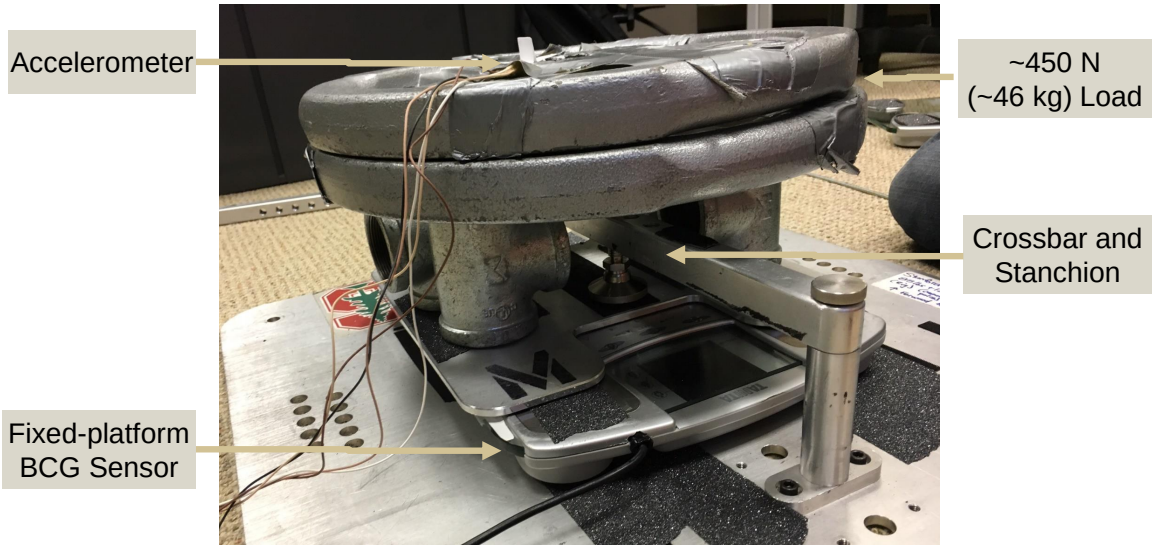

Figure 3.12: Photo of mechanical impulse response test setup.

In order to induce and record an impulse response, an accelerometer was placed on the scale along with a constant $\sim$ 450 N load as shown in Figure 3.12 above. Various crossbar preloads between 50 and 500 N were then employed. For each crossbar preload, a small rubber ball was dropped from a constant height onto the assembly to cause the impulse, and the accelerometer readings were recorded by a USB-6009 (National Instruments®, Austin, TX) ADC at 10 kHz. The average of five impulse responses was used for each crossbar preload in order to mitigate inconsistencies in the impulse process.

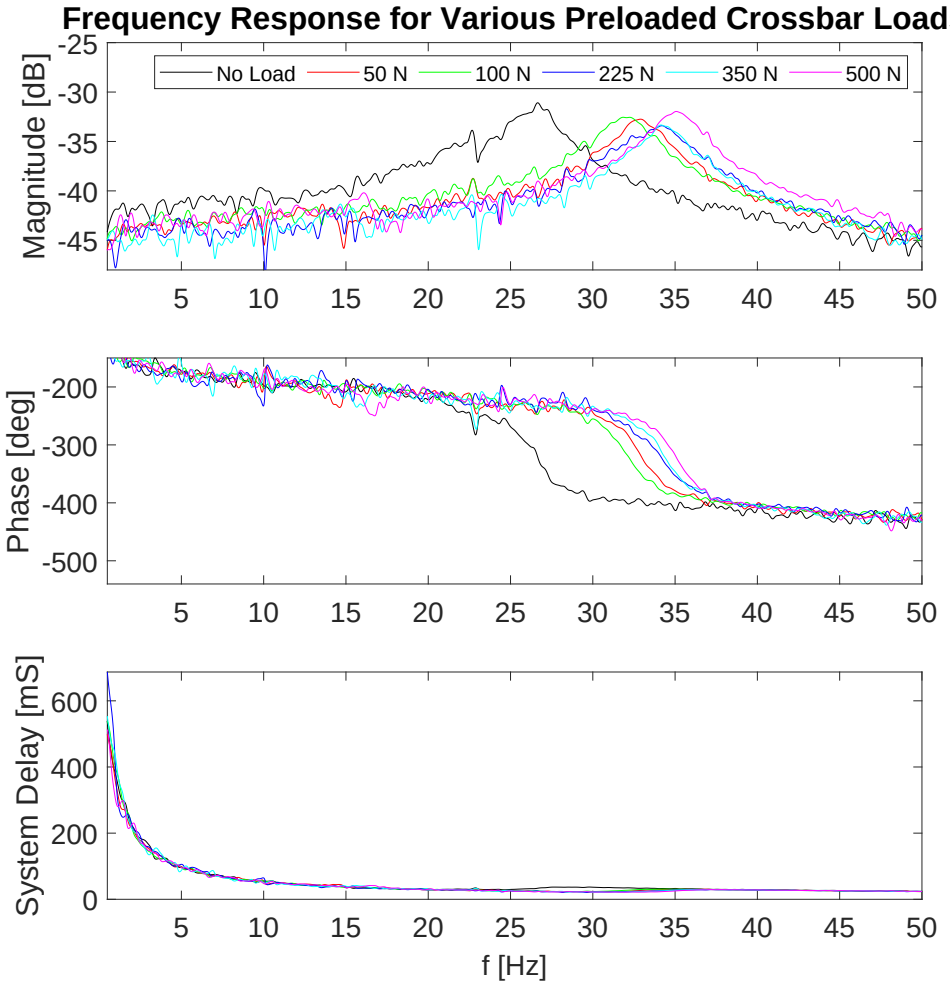

Figure 3.13: Frequency response of mechanical system derived from impulse response experiments (rows 1–2), and system delay calculated according to Equation 3.3 (row 3).

The first two rows in Figure 3.13 above show the results of 2^{20} point FFTs taken from 2^{15} sample (3.3 s) impulse responses using Hanning window smoothing. From the FFT, it was apparent that the frequency response of the system was indeed dependent on the crossbar preloading. In order to determine the error induced between no preloading and various preloads, the average magnitude and system delay was

measured from the frequency response between 3–10 Hz, where the BCG signal is most prominent [107, 108]. System delay here is defined as:

$$System\,Delay[f] = -\frac{1000 \cdot Phase[f]}{360 \cdot f} ms \tag{3.3}$$

where f is frequency, and $Phase[f]$ is the phase of the frequency response. The third row in Figure 3.13 above shows this system delay.

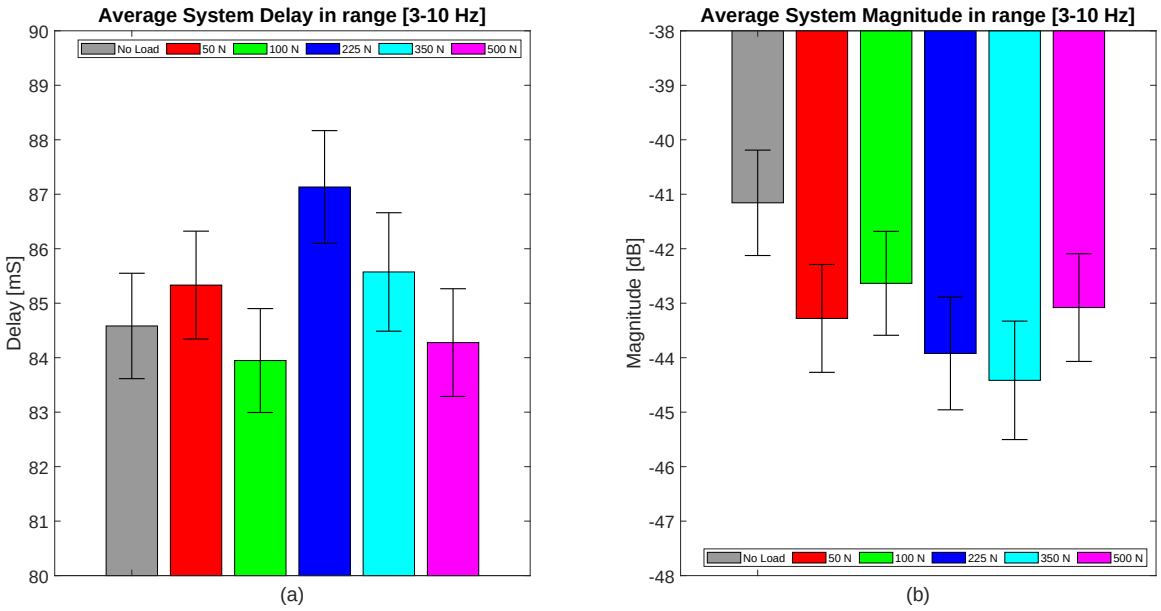

Figure 3.14: Average (a) system delay and (b) system magnitude for various preloads averaged over the 3–10 Hz frequency range where BCG is most prominent. Error bars show standard error.

Figure 3.14 above shows the average system delay and magnitude of the varying crossbar preloads within the 3–10 Hz bandwidth of interest. It is unknown why different crossbar preloadings resulted in different system delay and magnitude values, but it can be seen that the system delay at all various crossbar preloadings stayed within 4 ms of the system delay without the crossbar (no load). Therefore, it was concluded that, since 4 ms is within one sample period of the Shimmer®'s 256 Hz ADC sample rate, variable crossbar preloadings did not significantly effect the timing of the signal features within the BCG bandwidth. However, it can be seen that the

magnitudes with the crossbar preload were as much as 4 dB different compared to the magnitude without the crossbar preload, indicating that the crossbar preload did significantly affect the magnitude of the signal figures within the BCG bandwidth. Therefore, in the experiments in Chapters 4 and 5, signal magnitude comparisons were not made between measurements involving the crossbar preload.

3.6 Postprocessing

After signals were recorded, standard digital postprocessing was employed using various digital filters, ensemble averaging, and feature extraction methods. Digital filtering is discussed in Section 3.6.1, baseline removal and ensemble averaging is discussed in Section 3.6.2, and feature extraction is discussed in Section 3.6.3.

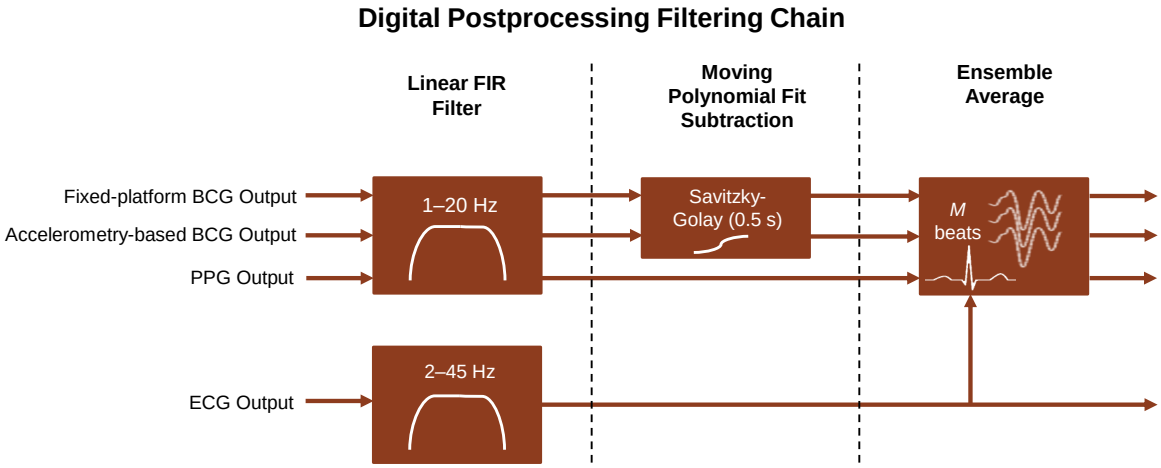

Figure 3.15: Block diagram of the digital postprocessing filter chain for Fixed-platform BCG, Accelerometry-based BCG, PPG, and ECG.

3.6.1 Standard BCG, ECG, and PPG Postprocessing

In addition to the analog electronic filters described in Sections 3.2 and 3.3, digital filters were also employed before data analysis and feature extraction as described in Figure 3.15 above. For the fixed-platform BCG, accelerometry-based BCG, and

PPG, a 1–20 Hz digital FIR filter (Kaiser window, length of 1,429 samples, 80 dB attenuation) was employed. For the ECG, a 2–45 Hz digital FIR filter (Kaiser window, length of 858 samples, 80 dB attenuation) was employed.

3.6.2 Standard Baseline Removal and Ensemble Averaging

Even after analog and digital filtering, non-frequency-based filtering could still be used to further reduce in-band noise. For example, in the case of the BCGs, movement was a common source of noise, particularly in microgravity where subjects were unfamiliar and attempted to move around to "balance" themselves. This was an issue when the movement was inside of the 1–20 Hz inner frequency band of the filters because this noise would not be attenuated. In order to mitigate this noise, two strategies were employed. The first was a non-frequency based technique of baseline removal in which a 3rd order 0.5 s moving polynomial fit (Savitzky-Golay) was subtracted from the signal [109]. This was effective in removing a slowly changing baseline that was still too fast to be AC-coupled out by the 1 Hz high-pass filters.

The second strategy for removing in-band noise, ensemble averaging, used ECG R waves as fiducials to align BCG or PPG beats that occured at a constant time from electrical depolarization. In this way, multiple beats could be be averaged so that all non-periodic information was attenuated. In practice, this left only the physiological information (i.e., BCG waveform). Ensemble averaging was done by aligning each beat of a subject's recording to the corresponding ECG R wave peak in a matrix:

$$X[n] = \begin{bmatrix} x_1[n] \\ x_2[n] \\ \vdots \\ x_M[n] \end{bmatrix}, \qquad n = 1, \ldots, L \tag{3.4}$$

where X was a subject's beat matrix, M was the number of beats, and L was the sample length of each beat. In this study, L=217 (0.85 s), where the R wave peak

was aligned at n=27 (0.1 s). The ensemble average of X was then defined as:

$$EA(X)[n] = \frac{1}{M}\sum_{i=1}^{M} x_i[n], \qquad n = 1, \ldots, L \tag{3.5}$$

3.6.3 Feature Extraction

The main features of interest for the experiments in Chapters 4 and 5 were the RJ interval, PTT, and SNR. Additionally, the K wave timing of the fixed-platform BCG was also extracted for discussion. In all cases, the dataset was first partitioned to remove all irrelevant data (e.g., hypergravity, setup, and microgravity transitions) using the Shimmer® accelerometer. For example, a relevant segment that is one microgravity parabola is shown in Figure 3.1(b) on page 32. Notice the acceleration reading is constantly zero during this segment. Once the irrelevant sections were removed, feature extraction was employed on the remainder according to the following subsections.

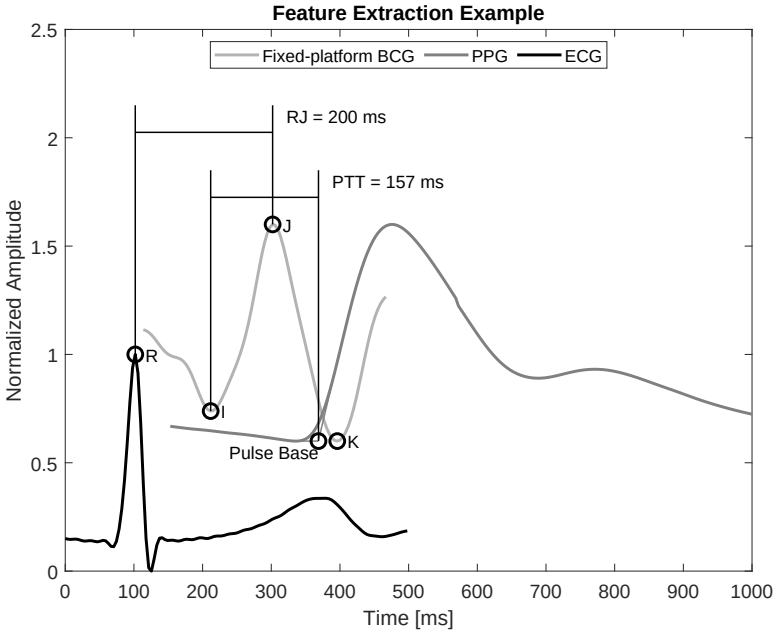

Figure 3.16: Feature extraction example showing timings used to calculate the RJ interval and PTT, as well as the K wave timing. Signals in the figure were manually truncated for clarity.

RJ Interval, PTT, and K wave Timings

In order to calculate the RJ Interval, PTT, and K wave timings, the individual timings of the R, I, J, and K waves were first determined. R waves were first automatically classified with a neural network-based algorithm [110]. The J wave was then determined as the largest peak between the R wave and the next 300 ms. The I and K waves were then manually determined as the first major trough before and after the J wave respectively. Next, the pulse base of the PPG was determined as the intersection of the tangents of the first trough and maximum first derivative of the waveform. With the timings calculated, the RJ interval was then defined as the time between the R and J waves, and the PTT was defined as the time between the I wave and the PPG pulse base. All of these timings and intervals are illustrated in Figure 3.16 above.

Signal-to-noise Ratio (SNR)

The SNR was estimated by calculating the average sample correlation coefficient SNR estimation between distinct pairs of sequential beats: $\{(x_1, x_2), (x_3, x_4), \ldots, (x_{M-1}, x_M)\}$. This method, summarized below, provides an unbiased SNR estimation when there is a large number of pairs [111].

For each pair (x_j, x_k), the sample correlation coefficient, r, was defined as:

$$r = \frac{\frac{1}{L}\sum_{n=1}^{L}(x_j[n] - \overline{x_j})(x_k[n] - \overline{x_k})}{\sqrt{\frac{1}{L}\sum_{n=1}^{L}(x_j[n] - \overline{x_j})^2 \frac{1}{L}\sum_{n=1}^{L}(x_k[n] - \overline{x_k})^2}} \tag{3.6}$$

where $\overline{x}$ denoted the average value of vector x. The SNR estimate, SNR_r, was then defined as:

$$SNR_r = A\frac{r}{1-r} + B \tag{3.7}$$

for constants A and B as given in [111]:

$$A = \exp(\frac{-2}{L-3}), \qquad B = -\frac{1}{2}(1 - \exp(\frac{-2}{L-3})) \tag{3.8}$$

Negative SNR_r values were set to zero before averaging. For SNR comparisons, only

the first M beats in each dataset were included, where M was the smaller of the two dataset sizes.

3.7 Discussion

Despite fulfilling the seven requirements in Section 3.1, the designs presented in this chapter could still be improved in future work. The limitations and suggested improvements for the instrument are discussed in the following sections.

3.7.1 Limitations

The largest limitation of the current design was that in order to record accurate fixed-platform BCG amplitudes, the instrument needed to be recalibrated every time the securing crossbar and stanchion were adjusted, as discussed in Section 3.5.4. During parabolic flight, the crossbar and stanchion were removed and reassembled every flight, making amplitude comparisons between flights not possible. With a permanently mounted instrument, such as on a spacecraft, the securing crossbar and stanchion may never need to be removed, negating this problem. However, the effectiveness of the parabolic flight experiments was limited because of this. For example, cardiac output trending between parabolic flights was not possible because this relies on amplitude measurements of the fixed-platform BCG as discussed in Section 2.1.2.

Another limitation of the current design was that the fixed-platform BCG was only one-dimensional (longitudinal). Considering that BCG is inherently a three-dimensional signal [112], significant information may be lost when measuring it along only a single axis [70]. Despite this, the correlation studies discussed in Sections 2.1.1–2.1.4 still validate longitudinal fixed-platform BCG measurement for the four target parameters in this dissertation.

The final major limitation of this instrument was the use of a commodity bathroom scale as the core sensor. Although the scale used in this dissertation was previously validated for robust fixed-platform BCG acquisition with a bandwidth up to 10 Hz

[81], it may have also been useful to have a larger bandwidth available to measure the "true" BCG waveform instead of just enough to calculate the features discussed in this dissertation.

Overall, the instrument discussed in this dissertation was capable of measuring trends in the four target parameters discussed in Chapters 1 and 2, so long as the instrument was not disassembled between measurements. If it was, only trends in contractility, arterial stiffness, and blood pressure could be measured (not cardiac output), unless the crossbar and stanchion are redesigned or reconfigured to apply a constant preload between assembly procedures.

3.7.2 Suggested Design Improvements for Future Work

In order to overcome the limitations listed in Section 3.7.1, future work should base the fixed-platform BCG sensor design on a high-bandwidth force plate instead of a commodity bathroom scale. It has been shown that parameters such as contractility and stroke volume are slightly more accurate when measured on a high-bandwidth force plate compared to the scale used in this dissertation [113]. Additionally, the crossbar and stanchion would not be required to preload the scale since the force plate can measure in both compression and tension directions. This eliminates the recalibration on reassembly problem and bandwidth limitations of the current design. It could also perform a three-axis measurement.

Another improvement to the design would be the addition of in-band vibration cancellation using adaptive filtering such as that presented in [83]. In the experiments in this dissertation, high-quality signals were recorded using mechanical vibration isolation, analog filtering, and digital filtering, but signal quality could still have been improved further with the addition of adaptive filtering.

An additional research topic that could be explored is the development of a gravity-dependent transfer function between fixed-platform BCG measurements taken in normal gravity, and measurements taken at varying gravity levels (e.g., Mars, Moon, or microgravity). If such a transfer function were developed, the innate changes to the BCG morphology due to gravity changes could be filtered out, and the resulting BCG

could be analyzed using all of the clinical knowledge of BCG that has been studied on Earth since the late 19th century.

3.8 Conclusions

This chapter presented the instrument designs used in this dissertation for fixed-platform BCG, accelerometry-based BCG, ECG, and PPG measurement. The design fulfilled the two core and five research system requirements described at the beginning of this chapter, and was more practical than other microgravity BCG sensing devices in that it does not require uninterrupted free-float to function. Although it was capable of measuring the four target parameters discussed in Chapters 1 and 2, its main limitation was that it could not be disassembled and reassembled without requiring amplitude recalibration. This limited its ability to be used for cardiac output trending across multiple parabolic flights.

Chapter 4

Human Parabolic Flight Experiment: Signal Quality Validation and Comparison to Accelerometry-based BCG

The work described in Chapter 3 resulted in a design that fulfilled the target system requirements by encompassing an instrument capable of measuring trends in the four target parameters in a confined microgravity space by means of measuring fixed-platform BCG and toe PPG. The validation discussed in this chapter shows that the instrument could successfully measure these two signals in a population of subjects aboard confined parabolic flight vehicles. It also shows that the signal quality of the measured fixed-platform BCG was superior to that of the closest alternative, accelerometry-based BCG, in terms of SNR. Preliminary results from these experiments were published in [114], and partial results were published in [115, 116]. This chapter is the first time that data from all test subjects has been discussed in context together.

4.1 Introduction

As discussed in Chapter 2, BCG, combined with PPG, is an effective way to measure spaceflight-induced cardiovascular deconditioning. Previous works on microgravity BCG measurement have been focused on accelerometry-based approaches that require the subject to be suspended in uninterrupted free-float [69,70], which is not possible in confined spacecraft such as currently proposed DSTs or partial-gravity environments. The platform-based approach in this dissertation addressed this issue by providing a robust solution for BCG measurement using the same type of device that has been validated in several clinical studies on Earth discussed in Sections 2.1.1–2.1.4. In order to validate this approach in a relatively realistic environment, and compare the quality of the platform-based approach with that of the accelerometry-based approach, the platform-based instrument was deployed aboard a space-constrained parabolic flight vehicle in which 15 unique subjects were measured. The hypotheses of this experiment were: (1) the instrument is able to successfully measure the BCG and PPG features required for calculating the target parameters, and (2) compared to the accelerometry-based BCG approach, the platform-based approach yields a higher quality signal.

4.2 Materials and Methods

The fixed-platform BCG and PPG, along with the support devices developed in Chapter 3 (e.g., ECG, data logging electronics), were tested aboard two parabolic flight aircrafts. The experiment took place in the summers of 2013 and 2014 at NASA's Reduced Gravity Office, Johnson Space Center (Ellington Field), Houston, TX. Human subject test protocols were approved by the NASA and Stanford Institutional Review Boards protocols #CR00000337 and #24294 respectively.

Table 4.1: Population Demographics and Resting Vitals

Subject	**Sex**	**Age [years]**	**Weight [kg]**	**Height [cm]**	**Blood Pressure (Rest) [mmHg]**	**Heart Rate (Rest) [BPM]**
1	F	40	61	168	107 / 66	58
2	M	56	88	175	110 / 62	57
3	F	19	70	170	103 / 59	80
4	F	19	59	170	88 / 53	58
5	M	36	68	175	110 / 68	49
6	M	52	68	175	130 / 69	64
7	F	30	67	175	111 / 69	52
8	M	41	70	183	110 / 68	65
9	M	24	73	183	103 / 72	78
10	M	28	82	178	109 / 69	75
11	F	23	58	178	95 / 56	65
12	M	42	70	183	110 / 65	45
13	M	37	86	178	114 / 79	77
14	M	53	68	175	124 / 71	70
15	M	25	73	183	109 / 71	92
16	M	46	83	173	136 / 79	73
17	M	30	82	178	111 / 68	66
18	M	26	129	196	121 / 73	69
19	F	25	61	168	99 / 78	90
Mean		34.3	74.5	177.1	110.5 / 68.2	67.5
Std. Dev.		11.6	16.0	6.7	11.4 / 7.1	12.8
Coeff. Of Var.		33.8%	21.5%	3.8%	10.3% / 10.4%	19.0%

4.2.1 Subject Population

Nine healthy males (ages 24–56, mean 38.1) and six healthy females (ages 19–40, mean 26) participated in the study as shown in Table 4.1 above. The group was split

into two cohorts. The first, subjects 1–10, flew in 2013, and the second, subjects 11–19, flew in 2014. Four subjects were a part of both cohorts: Subject 6 is the same person as Subject 14, 8 as 12, 9 as 15, and 10 as 17. Age, weight, height, blood pressure, and heart rate for these subjects were reported individually each year.

4.2.2 Experiment Setup and Measurement Protocols

The 2013 cohort experiments took place on a Boeing 727-200 (Zero Gravity Corporation, Vienna, VA), and the 2014 cohort experiments took place on a McDonnell Douglas C-9B Skytrain II (NASA, Washington, D.C.). In order to prevent motion sickness, subjects were instructed not to eat the day of the flight, and were administered scopolamine orally or by rapid injection immediately before the flight (about 60-90 minutes before the experiment). The dosage of scopolamine was determined by the Flight Surgeon based on sex, weight, and prior experience in microgravity.

The cabin of the aircraft was configured to be mostly empty to leave room for experiments, except for a small seating section in the rear. During taxi, takeoff, and ascent, subjects were secured in standard airliner seats, and the instrument and

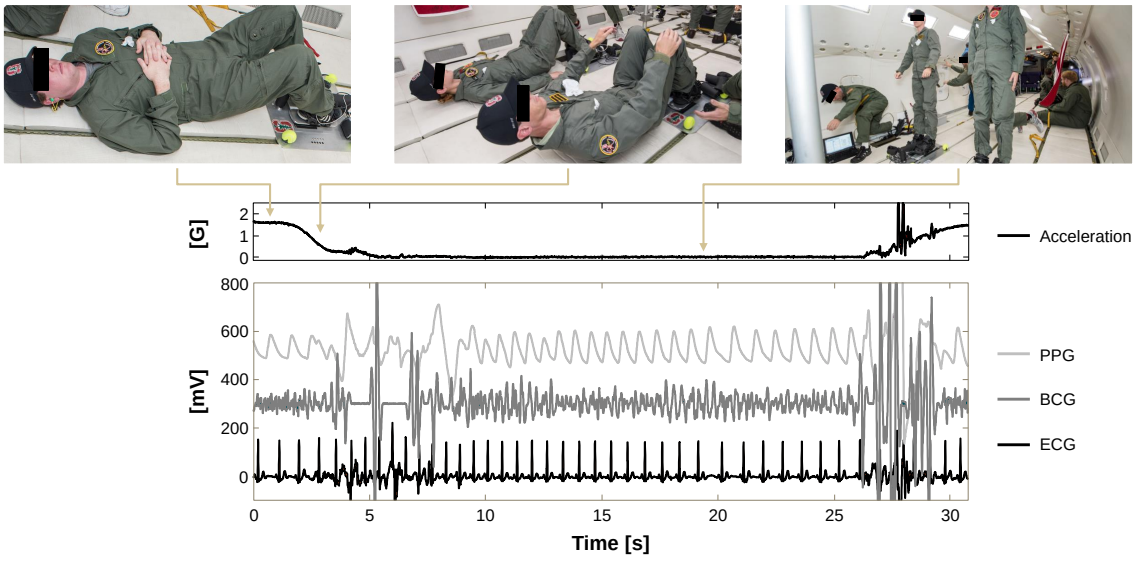

Figure 4.1: Measurement procedure for fixed-platform BCG in microgravity.

support equipment were stored disassembled in a cargo container. Once above 10,000 ft, the instrument and support equipment were assembled, setup, and tested. Once operational, each subject participated in a series of 14-20 parabolic maneuvers, each lasting approximately 17 seconds, to measure the fixed-platform and accelerometry-based BCG, along with ECG and PPG. Accelerometry-based BCG was only measured in the first cohort, and PPG was only measured in the second cohort.

Fixed-platform BCG was measured first. Before these measurements, subjects were instructed to lay down while strapped into the instrument until the microgravity segment, as shown in the top left of Figure 4.1 above. This was for safety during the hypergravity segments, and also to minimize fluid shift to the legs during all non-microgravity segments. When the microgravity segment was starting, the subject could easily move themselves upright with their leg muscles and stabilize as shown in the top center of Figure 4.1 above. Once stabilized, the subject remained in the measurement position as shown in the top right of Figure 4.1 above until instructed to lay back down for the upcoming hypergravity segment. This was repeated for every parabola.

Figure 4.2: Measurement procedure for accelerometry-based BCG.

After about 10 parabolas of fixed-platform BCG measurement, the remaining parabolas were used to measure accelerometry-based BCG. During these measurements, the subject was paired with a crew member on the research team to manipulate them as shown on the left in Figure 4.2 above. Before the microgravity segment, the subject laid on the ground holding onto a floor mounted rope for support. Once the microgravity segment started, the subject or their paired crew member pushed them up slightly from the floor before the crew member decelerated them to free-float still while disturbing them as little as possible as shown in Figure 4.2 above. Before the hypergravity segment, the paired crew member pulled the subject back down.

During all measurements, a dedicated research team crew member monitored the measurements in real time from a laptop in order to look for corrupt signals and ensure that the PPG gain did not need to be adjusted. If any issues were detected, electronics hardware was adjusted or swapped out with spare equipment so that the remaining parabolas could still be utilized.

Table 4.2: SNR_r Measurements and Difference Calculations

Subject	**Accelerometry-based BCG (longitudinal)**	**Fixed-platform BCG**	**Difference Factor**
1	0.32	0.69	2.13
2	0.21	0.60	2.86
3	0.92	0.99	1.08
4	0.26	1.02	3.91
5	0.20	0.92	4.50
6	0.68	0.36	0.53
7	0.76	0.22	0.29
8	0.36	0.42	1.15
9	0.29	0.71	2.44
10	0.35	0.65	1.87
Mean	0.44	0.66	2.08
Std. Dev.	0.25	0.27	1.39
Coeff. Of Var.	58.0%	40.9%	67.1%

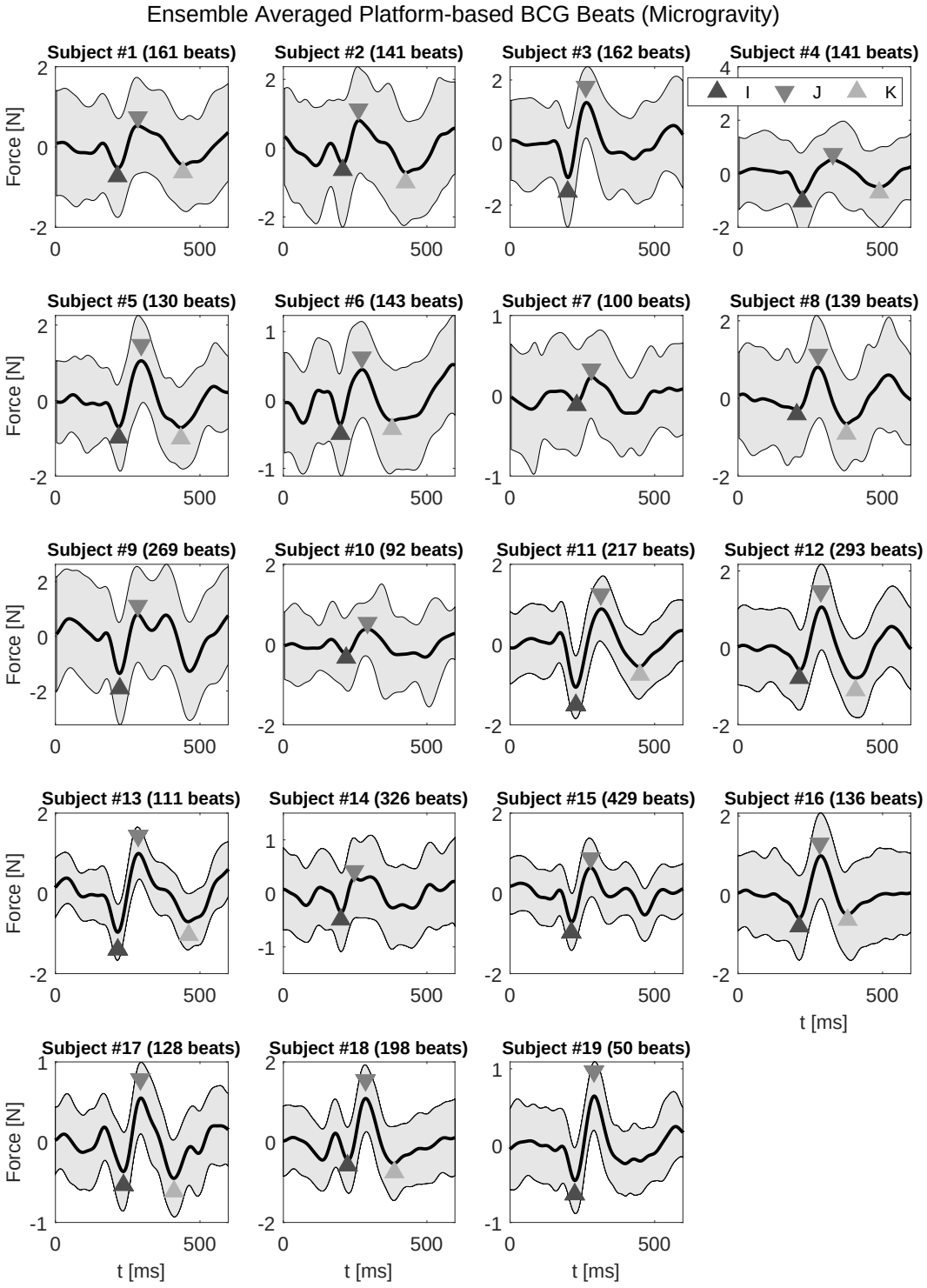

Figure 4.3: Fixed-platform BCG measured in microgravity for all subjects. Annotations show I, J, and K waves. The shaded area indicates +/– one standard deviation of the ensemble average at every point.

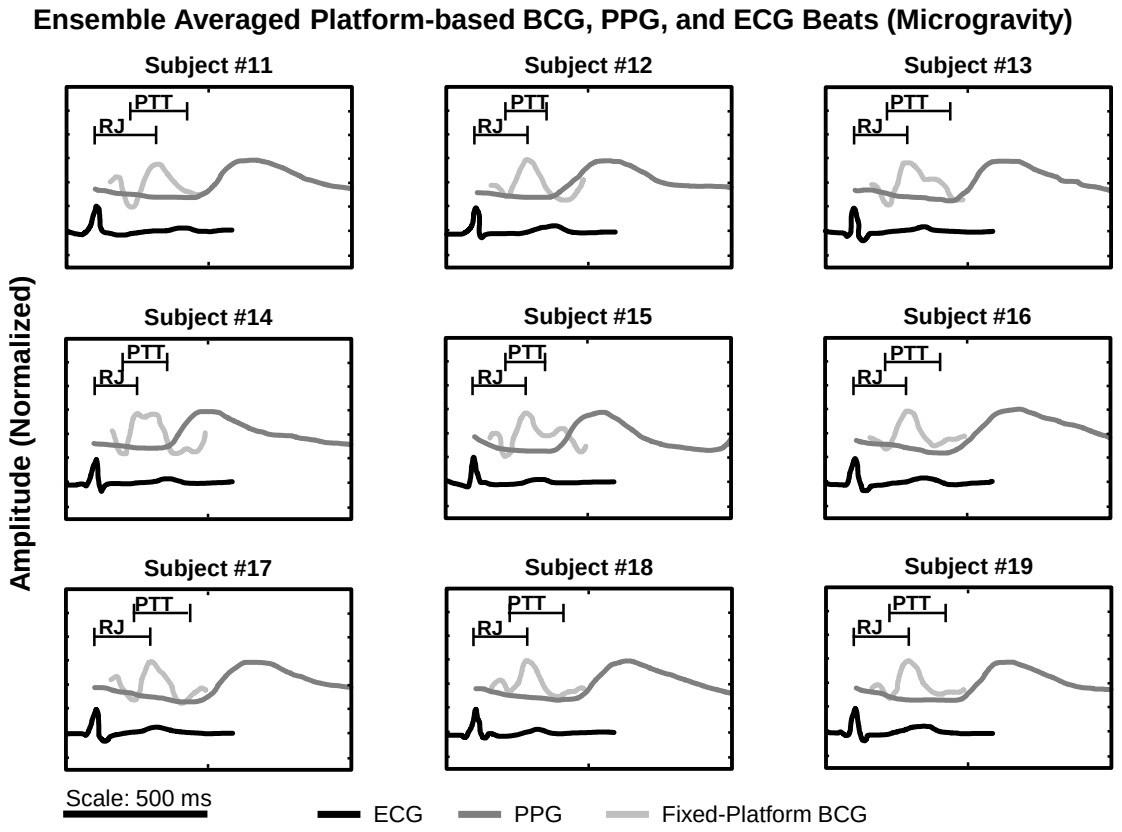

Figure 4.4: Fixed-platform BCG, PPG, and ECG measured in microgravity for the second cohort (Subjects 11–19). Annotations show the RJ interval and PTT timings.

4.3 Results

The measured fixed-platform BCG for all 19 subjects is shown in Figure 4.3 on the previous page. In all cases, the I and J waves could be distinguished, and in 12 of 19 cases, the K wave could be distinguished as well. The measured PPG alongside ECG and fixed-platform BCG for all subjects whose PPG was measured (cohort 2) is shown in Figure 4.4 above. RJ intervals and PTTs are also indicated in this figure for all subjects according to the feature extraction method discussed in Section 3.6.3. These two figures show that fixed-platform BCG and toe PPG were successfully measured in all subjects, and that the RJ-interval and PTT timings were able to be extracted.

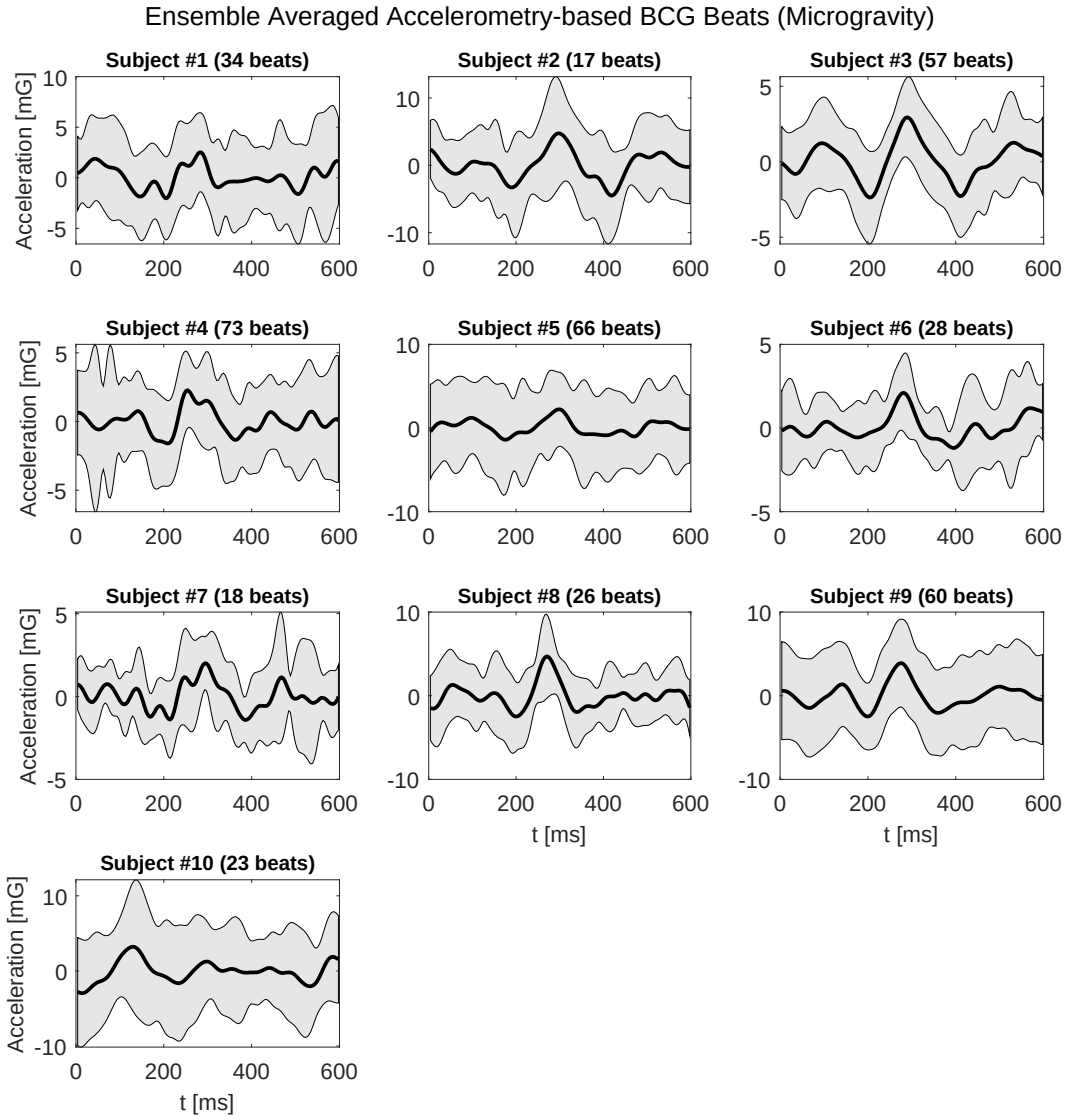

Figure 4.5: Accelerometry-based BCG measured in microgravity for the first cohort (Subjects 1–10). The shaded area indicates +/− one standard deviation of the ensemble average at every point.

The SNR_r for longitudinal (single-dimension) accelerometry-based and fixed-platform BCG for each subject whose accelerometry-based BCG was measured (cohort 1) is shown in Table 4.2 on page 60. SNR_r was calculated using the sample correlation coefficient method in Section 3.6.3. The measured accelerometry-based BCG for all

subjects whose accelerometry-based BCG was measured (cohort 1) is shown in Figure 4.5 above. In 8 out of 10 subjects, the SNR_r increased from accelerometry-based to fixed-platform BCG with an average overall difference factor of 2.08 (standard deviation = 1.39). When compared to the three-dimensional accelerometry-based BCG magnitude, the fixed-platform BCG SNR was increased, on average, by a factor of 5.44 (standard deviation = 4.52).

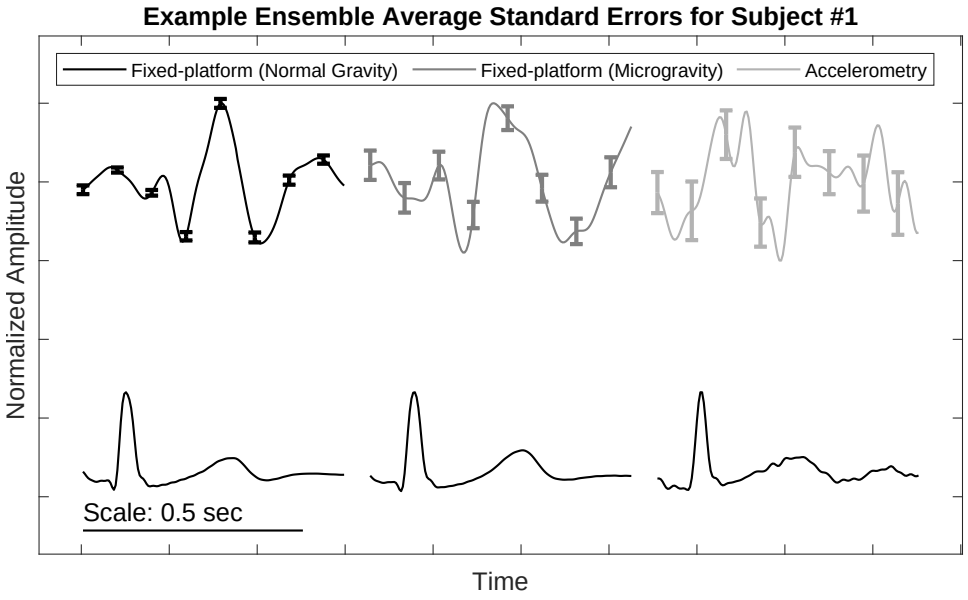

Figure 4.6: Single-subject example comparing the quality of BCG measured by the fixed-platform method in normal gravity (top left) and microgravity (top center), and by the accelerometry-based method while free-floating (top right). Error bars indicating quality show the standard error at several points of the ensemble average.

4.4 Discussion

The results in this chapter showed that fixed-platform BCG and PPG can indeed be measured in the confined environment of parabolic flight, and that the signals were of high enough quality to extract RJ interval and PTT timings for all subjects who were measured. Additionally, in most cases (12 of 19 subjects), the K wave timing of the fixed-platform BCG could be identified as well. The RJ interval and PTT

timings enable the instrument to measure trends in three of the four target parameters: contractility, arterial stiffening, and blood pressure. Unfortunately, because of inconsistent amplitude calibration between instrument reassemblies discussed in Section 3.5.4, cardiac output trending is not possible in the current configuration of the instrument. However, on an actual spaceflight vehicle or permanent installation, disassembly and reassembly during the mission may not be required, negating this limitation entirely and enabling measurement of all four target parameters without modifying the current version of the instrument.

The results also show that the fixed-platform BCG in microgravity yielded higher SNR compared to the accelerometry-based method in 8 of the 10 subjects tested. This is further illustrated by example in Figure 4.6 above, where standard error bars are shown for the ensemble averaging of fixed-platform BCG in normal gravity (left) and microgravity (center), as well as for accelerometry-based BCG (right) for a single subject. Error bars are larger from fixed-platform BCG in normal gravity to microgravity, likely because of motion noise of the microgravity subject trying to stabilize themselves. Error bars are also larger from fixed-platform BCG in microgravity to accelerometry-based BCG, likely because of the same motion noise being present, with the additional noise of collisions with the cabin walls and the research team crew member occasionally repositioning them.

Overall, the dataset from this experiment demonstrated the robustness of the platform-based approach for BCG monitoring, and positioned it as a viable solution for hemodynamic monitoring of astronauts on extended missions where cardiovascular alterations may result, and accelerometry-based BCG may be too difficult or impractical. With a tethered platform-based system as described in this dissertation, astronauts can simply maneuver to the scale platform, quickly latch their feet into the foot bindings, and be securely measured without constantly attempting to avoid free-floating collisions. Unlike accelerometry-based BCG, such a system can also be used in fractional-gravity environments such as the Moon or Mars.

4.4.1 Limitations of Experiment

The main limitation of this experiment is that it was not tested in any actual DST environments. Human microgravity experiments on DSTs are not possible at the current time, so it was instead decided to experiment on parabolic flight. In an actual DST, a more realistic cabin form factor could be tested, as well as longer duration microgravity. Without longer duration microgravity testing, it is not possible to validate the performance of the instrument for any duration of actual space travel, since longer than transient exposure to microgravity may impact the nature of fixed-platform BCG and PPG waveforms.

4.4.2 Future Work

Since it is not possible to experiment with actual DSTs yet, future work should focus on an experiment with longer term exposure to microgravity. For example, the instrument could be tested on the ISS. This would yield a stronger conclusion about how well fixed-platform and accelerometry-based BCG performs practically in a more realistic setting, and also answer questions about how longer term exposure to microgravity effects the fixed-platform BCG and PPG waveforms.

4.5 Conclusions

In this chapter, it was shown that the human parabolic flight experiment validated the performance of the instrument designed in Chapter 3, in that (1) the instrument was able to successfully measure the BCG and PPG features required for calculating the target parameters, and (2) compared to the accelerometry-based BCG approach, the platform-based approach yielded a higher quality signal. The major limitation of this experiment was that it was not performed in a DST. Future work should be focused on replicating this experiment during actual spaceflight (e.g., aboard ISS) in order to evaluate the fixed-platform BCG and PPG waveforms after longer term exposure to microgravity, then eventually aboard an actual DST in order to evaluate the instrument's practicality in a more realistic environment.

Chapter 5

Multi-gravity Experiment: Detection of Microgravity-induced Hemodynamic Changes

The validation started in Chapter 4 was extended to show that in addition to high quality static signals, relevant physiological change could also be measured. This was shown as changes in timings between defined waveform features between microgravity and normal gravity. As in Chapter 4, preliminary results from these experiments were published in [114], and partial results were published in [115, 116]. This chapter and Chapter 4 are the first time that data from all test subjects has been discussed in context together.

5.1 Introduction

It was validated in Chapter 4 that fixed-platform BCG and PPG can be measured in a confined microgravity environment, and that the quality of the fixed-platform BCG signal was higher than its closest alternative, accelerometry-based BCG. The next logical step in validating the instrument was to test whether physiological change relevant to cardiovascular deconditioning could be measured. To accomplish this, normal gravity measurements with the same instrument were also included in the data

collection. In this way, changes induced by microgravity relative to normal gravity could be measured. This was done in place of measuring during actual long-duration spaceflight, where cardiovascular deconditioning would eventually occur, since actual spaceflight experiments are not feasible at this time and are left to future research. The hypothesis of this experiment was that the instrument is sensitive enough to measure expected hemodynamic changes induced by microgravity with respect to normal gravity.

5.2 Materials and Methods

The same fixed-platform BCG, PPG, support devices, parabolic flight campaigns, and IRB protocols that were tested in Chapter 4 were also used in these experiments. The difference is that additional fixed-platform BCG and PPG measurements were taken in normal gravity after landing as well as during flight.

5.2.1 Subject Population

The same two cohorts of subjects participated in this study, as shown in Table 4.1 on page 57. As in the previous experiment, only those in the second cohort, subjects 11–19, had their PPG measured. Both cohorts had their fixed-platform BCG measured.

Figure 5.1: Measurement position for fixed-platform BCG in normal gravity.

5.2.2 Experiment Setup and Measurement Protocols

The experiment took place on the same two parabolic flight aircraft described in Chapter 4. The protocol for the microgravity measurements is described in Section 4.2.2. For normal gravity measurements, subjects were first allowed to rest sitting down for five minutes, then their resting vitals, shown in Table 4.1 on page 57, were recorded. The subjects were then measured while standing on the fixed-platform BCG sensor with the PPG sensor still attached, as shown in Figure 5.1 above.

Before flight, subjects were administered scopolamine orally or by rapid injection immediately before the flight (about 60-90 minutes before the microgravity measurements) in order to help prevent motion sickness. Scopolamine is a muscarinic cholinoceptor blocking agent that blocks some of the effects of acetylcholine (a neurotransmitter) within the nervous system, inhibiting the vomiting center of the parasympathetic nervous system. Scopolamine's affect on the cardiovascular system has been

studied. In a population of nine men (ages 28-59, mean 51.1), it was shown that brachial and ankle mean arterial pressure does not significantly change, and that brachial-ankle PWV was increased very slightly 30 minutes after injection, but was not significantly changed 60 minutes after injection [117]. Therefore, it was unlikely that scopolamine itself had any significant effect on the measurements in this experiment, and any effect during microgravity measurements would have also been present during normal gravity measurements.

5.2.3 Statistical Approach

In order to compare a subject's measurement in normal gravity to their measurement in microgravity, a single-tailed paired T-test was used to determine if there was a statistically significant difference between these two configurations. P-values less than or equal to 0.05 were considered significant, and reported in Section 5.3. In cases where a subject participated twice in the population (they were present in both 2013 and 2014 cohorts), both a P-value for 19 participants as well as for 15 unique participants was reported. In this case, subjects in both cohorts are only counted in the first cohort. In cases where data was missing (i.e., the K wave was not distinguishable), the subject was removed from the dataset when the missing data was relevant.

Correlations between subject demographics and changes to defined waveform features induced by microgravity were also calculated using standard linear regression analysis. For correlations with binary demographic variables (i.e., sex), the Point-Biserial method was used to calculate the correlation coefficient, R_{pb}. Correlation coefficients of more than or equal to $R^2 = 0.4$ were considered significant, and reported in Section 5.3.

5.3 Results

The first statistically significant hemodynamic change detected was a decrease in RJ interval from normal gravity to microgravity ($P = 4 \times 10^{-7}$ for all subjects and

$P = 7 \times 10^{-6}$ for 15 unique subjects). The average change was 35.8 ms with a standard deviation of 21.4 ms. These RJ intervals are shown in Table 5.1 below.

Table 5.1: RJ Interval Changes From Normal Gravity to Microgravity

Subject	**Sex**	**Age [years]**	**Weight [kg]**	**Height [cm]**	**Normal Gravity [ms]**	**Micro-gravity [ms]**	**Diff-erence [ms]**
1	F	40	61	168	214.8	179.7	-35.1
2	M	56	88	175	210.9	156.2	-54.7
3	F	19	70	170	203.1	156.2	-46.9
4	F	19	59	170	207.0	226.5	19.5
5	M	36	68	175	257.8	195.3	-62.5
6	M	52	68	175	203.1	167.9	-35.2
7	F	30	67	175	218.7	179.6	-39.1
8	M	41	70	183	210.9	171.8	-39.1
9	M	24	73	183	250.0	179.7	-70.3
10	M	28	82	178	214.8	191.4	-23.4
11	F	23	58	178	219.6	211.8	-7.8
12	M	42	70	183	200.0	184.3	-15.7
13	M	37	86	178	223.5	184.3	-39.2
14	M	53	68	175	200.0	145.1	-54.9
15	M	25	73	183	196.1	180.4	-15.7
16	M	46	83	173	223.5	180.4	-43.1
17	M	30	82	178	223.5	192.2	-31.3
18	M	26	129	196	243.1	184.3	-58.8
19	F	25	61	168	215.7	188.2	-27.5
Mean		34.3	74.5	177.1	217.7	181.9	-35.8
Std. Dev.		11.6	16.0	6.7	16.9	18.7	21.4
Coeff. Of Var.		33.8%	21.5%	3.8%	7.8%	10.3%	59.8%

Table 5.2: PTT Changes From Normal Gravity to Microgravity

Subject	**Sex**	**Age [years]**	**Weight [kg]**	**Height [cm]**	**Normal Gravity [ms]**	**Micro-gravity [ms]**	**Diff-erence [ms]**
11	F	23	58	178	172.7	243.3	70.6
12	M	42	70	183	156.9	180.5	23.6
13	M	37	86	178	141.3	251.1	109.8
14	M	53	68	175	145.2	164.8	19.6
15	M	25	73	183	149.2	172.7	23.5
16	M	46	83	173	157.0	235.5	78.5
17	M	30	82	178	153.0	243.4	90.4
18	M	26	129	196	188.4	235.5	47.1
19	F	25	61	168	160.9	239.5	78.6
Mean		34.1	78.9	179.1	158.3	218.5	60.2
Std. Dev.		10.8	21.1	7.9	14.6	34.9	32.9
Coeff. Of Var.		31.7%	26.7%	4.4%	9.2%	16.0%	54.7%

The second statistically significant hemodynamic change detected was an increase in PTT from normal gravity to microgravity ($P = 3 \times 10^{-4}$ for all subjects measured). The average change was 60.2 ms with a standard deviation of 32.9 ms. These PTT intervals are shown in Table 5.2 above. This table only includes subjects 11–19 since only the second cohort of subjects had their PPG, and thus PTT, measured.

Table 5.3: IJ and JK Interval Changes From Normal Gravity to Microgravity

Subject	IJ Interval Normal Gravity [ms]	IJ Interval Micro-gravity [ms]	Diff-erence [ms]	JK Interval Normal Gravity [ms]	JK Interval Micro-gravity [ms]	Diff-erence [ms]
1	85.9	70.4	-15.5	89.9	156.2	66.3
2	89.8	54.7	-35.1	85.9	164.1	78.2
3	93.8	62.5	-31.3	117.2	–	–
4	82.0	105.4	23.4	97.7	160.2	62.5
5	109.4	78.1	-31.3	97.6	136.7	39.1
6	93.8	74.2	-19.6	70.3	105.5	35.2
7	82.0	50.7	-31.3	105.5	–	–
8	78.1	74.2	-3.9	85.9	97.7	11.8
9	78.2	62.5	-15.7	97.6	–	–
10	85.9	74.2	-11.7	101.6	–	–
11	86.3	86.2	-0.1	100.3	135.5	35.2
12	90.2	74.5	-15.7	96.4	120.0	23.6
13	90.2	70.6	-19.6	84.7	174.6	89.9
14	90.2	47.1	-43.1	73.0	–	–
15	74.5	66.6	-7.9	112.2	–	–
16	98.0	70.6	-27.4	76.8	96.5	19.7
17	90.2	58.8	-31.4	–	116.1	–
18	94.1	62.8	-31.3	135.4	100.4	-35.0
19	82.3	66.7	-15.6	108.2	–	–
Mean	88.2	69.0	-19.2	96.5	130.3	38.8
Std. Dev.	8.1	13.1	15.4	16.2	28.2	35.0
Coeff. Of Var.	9.2%	19.0%	80.4%	16.8%	21.7%	90.4%

Aside from the RJ interval and PTT timings, statistically significant changes were also detected in the shape of the fixed-platform BCG waveform. There was an average decrease of 19.2 ms (standard deviation = 15.4 ms) in the IJ interval ($P = 2 \times 10^{-5}$ for all subjects and $P = 3 \times 10^{-4}$ for 15 unique subjects), there was an average increase of 38.8 ms (standard deviation = 35 ms) in the JK interval where K waves were distinguished ($P = 2 \times 10^{-3}$ for all subjects and $P = 3 \times 10^{-3}$ for 10 unique subjects), and there was an average increase of 22.8 ms (standard deviation = 41.4 ms) in the IK interval where k waves were distinguished ($P = 5 \times 10^{-2}$ for all subjects and $P = 6 \times 10^{-2}$ for 10 unique subjects). IJ and JK intervals are shown

in Table 5.3 above, and IK measurements can be calculated by adding IJ and JK intervals together.

Correlation coefficients were calculated between all demographic variables recorded (age, weight, height, body mass index, and sex) and changes to defined waveform features induced by microgravity (IJ interval, JK interval, IK interval, RJ interval, and PTT). Significant correlations are reported in Figures 5.2 and 5.3 below. The increase in IK interval was correlated with height (R^2=0.56), weight (R^2=0.44), and sex (R^2_{pb}=0.51). The increase in JK interval was correlated with height ($R^2 = 0.56$), and the decrease in RJ interval was correlated with sex ($R^2_{pb} = 0.41$). All other correlation coefficients were less than $R^2 = 0.4$.

5.4 Discussion

The results in Section 5.3 show that the the fixed-platform BCG and PPG can indeed measure physiological change induced by microgravity, as indicated by statistically significant changes to the RJ interval, PTT, and fixed-platform BCG waveform shape in microgravity with respect to normal gravity. In the case of the RJ interval, IJ interval, JK interval, and IK interval, this was shown across both cohorts with $P < 0.000001$, $P < 0.0001$, $P < 0.01$, and $P \leq .05$ respectively. In the case of PTT, this was shown across the second cohort that had their PPG measured with $P < 0.001$.

The likely physiological genesis of these changes is described in Section 2.3.1. In summary, compared to an upright position in normal gravity, parabolic flight induces a headward fluid shift similar to what would be experienced transitioning from an upright to a supine position. This increases venous return and thus cardiac output. Compared to a supine position in normal gravity, the microgravity phase of parabolic flight induces an expansion of the thoracic cage, unloading tissue pressure on the cardiovascular system within the thorax, as confirmed by a measured decrease in esophageal pressure [10]. The net effect of this is an increase in TCVP, further increasing venous return and cardiac output. It has also been shown that, despite this increase in cardiac output, mean arterial pressure does not change significantly, indicating that parabolic flight also induces vasodilation [23].

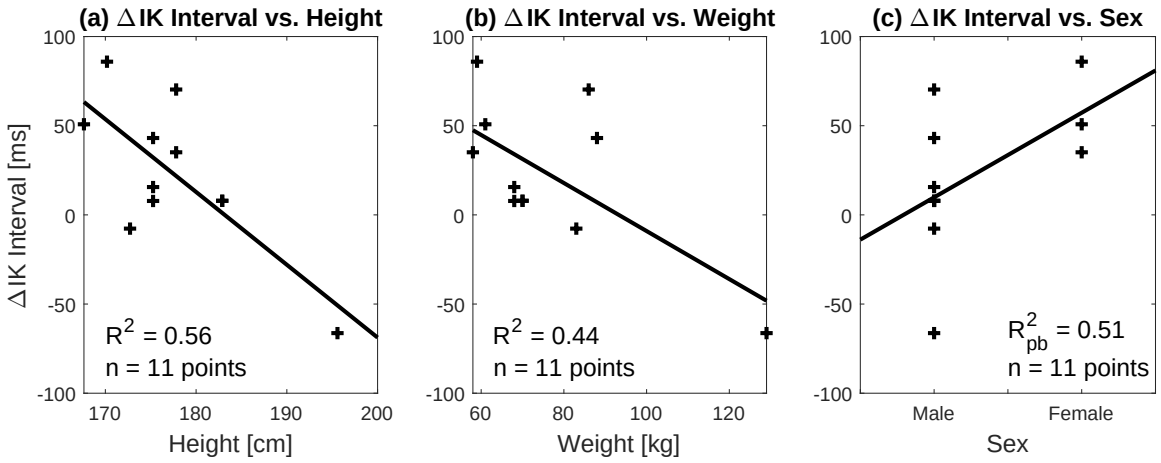

Figure 5.2: Change in IK interval vs. (a) height, (b) weight, and (c) sex. The solid black line shows the best least-squares regression for the data.

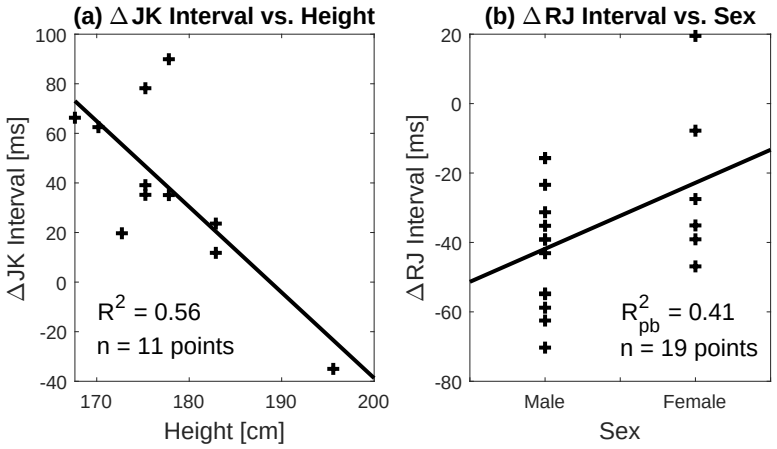

Figure 5.3: (a) Change in JK interval vs. height, and (b) change in RJ interval vs. sex. The solid black line shows the best least-squares regression for the data.

With respect to the RJ interval decrease, this was expected since it is correlated with PEP, and PEP is reduced with increased venous return. With respect to the PTT increase, this was also expected since it decreases with vasodilation (increased vessel radius and decreased elastic modulus) according to the related PWV equation (Equation 2.4).

With respect to the change in fixed-platform BCG shape (decreased IJ interval, increased JK interval, and increased IK interval), this represents an elongation of the IJK complex, with the J wave peaking sooner. One possible explanation for this is that the PTT within the aorta is actually decreased, as indicated by a shorter IJ interval according to Equation 2.1 [80]. In this case, the increased PTT observed in this experiment from the toe must have been dominated by the expected peripheral vasodilation rather than central PWV. Unfortunately, no known research has been done on central PWV during parabolic flight in order to verify this.

Moderate correlations (R^2 between 0.41 and 0.56) were found between several pieces of demographic data and changes to defined waveform features induced by microgravity. First, the increase in IK interval was negatively correlated with the height and weight of the subject (Figure 5.2(a) and (b) above). There was also a correlation between the increase in IK interval and sex (Figure 5.2(c) above), where males represented smaller changes. Considering that, in this study, males were also associated with larger heights and weights, this observation corresponds to larger bodies having had a smaller elongation of the fixed-platform BCG's IJK complex when they entered microgravity. Second, the increase in JK interval was negatively correlated with the height of the subject (Figure 5.3(a) above), with shorter subjects exhibiting a longer elongation of the JK interval when they entered microgravity. Notably, the tallest subject (Subject #18), was the only subject who experienced a negative change to their JK interval when they entered microgravity. Third, there was a correlation between the decrease in RJ interval and sex (Figure 5.3(b) above), where males represented larger decreases in RJ interval when they entered microgravity. The genesis of these demographic correlations is unknown and left to future work.

5.4.1 Limitations

There were two main limitations to this experiment not mentioned in previous chapters. The first was that the subject's orientation during the normal gravity reference was upright, while their orientation in microgravity was much more similar to supine

in terms of fluid arrangement. This results in the measurement of not only the effects of microgravity, but also the effects of a major postural difference.

The second limitation was that trends in the target parameters for the instrument were not actually calculated. For example, PTT-based blood pressure could have been calibrated for each subject in normal gravity, then results on microgravity-induced blood pressure changes may be able to be reported. Since none of the four target parameters were tracked directly in this experiment, their effectiveness using the instrument in this dissertation remains hypothetical.

5.4.2 Future work

In order to address the two limitations above, the following could be improved in future work: first, the normal gravity reference position should be supine. This would be very difficult to achieve with the current device design that requires standing on the sensor in normal gravity. Instead, the subject could lie on a hanging table, with their feet strapped into the sensor mounted vertically against a wall, similar to the table in [71]. This would allow for longitudinal measurement while in the supine position using the same sensor. Second, the fixed-platform BCG and PPG's relationship to the four target parameters could be calibrated for each subject so that changes in the four target parameters could be tracked in microgravity.

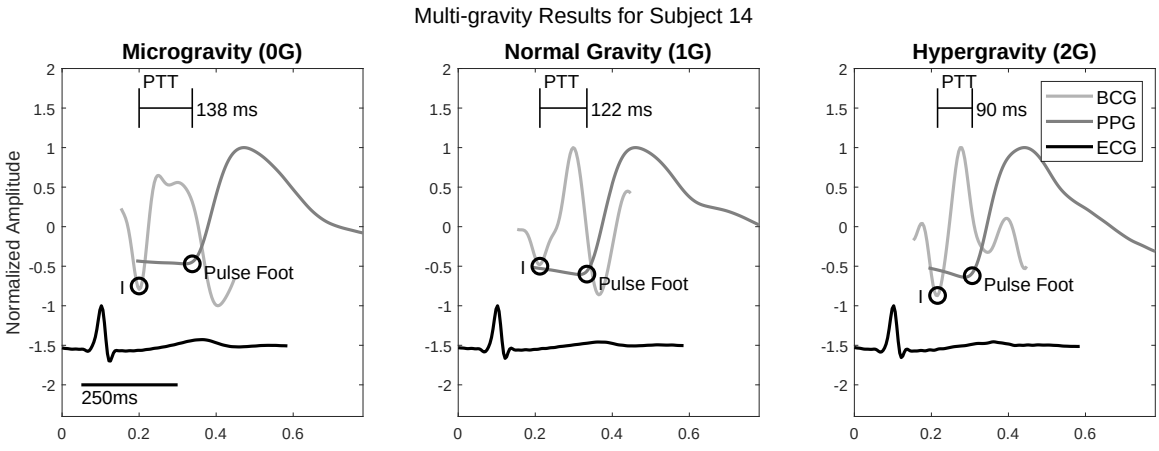

Figure 5.4: Fixed-platform BCG and PPG measurement of one subject during three gravity levels. As the gravity level increased, PTT decreased.

Another improvement that could be done in future work is recording measurements at multiple gravity levels. Parabolic flight is capable of microgravity, but also partial gravity (e.g., Lunar or Martian equivalent) and hypergravity. In the experiment in this chapter, only microgravity segments were utilized. However, one subject accidentally stayed standing on the fixed-platform BCG sensor while in hypergravity instead of lying down. This is shown in Figure 5.4 above. It can be seen in this anecdotal data that as the gravity level increased, PTT decreased. If more multi-gravity data were collected for multiple subjects, a mathematical relationship between gravity level and physiological change may be able to be determined.

5.5 Conclusions

In this chapter, it was shown that the instrument designed in Chapter 3 was sensitive enough to measure expected hemodynamic changes induced by microgravity with respect to normal gravity. The major limitations of this experiment were that orientation of the test subject changes between normal gravity and microgravity, and that the four target parameters were not explicitly reported. Future work should be focused on overcoming these limitations and collecting data in more than two gravity levels.

Chapter 6

Conclusion and Future Directions

6.1 Conclusions

The work described in this dissertation establishes the groundwork for a hemodynamic monitoring system capable of being used in deep space. With the novel instrument discussed in Chapter 3, trends in contractility, cardiac output, arterial stiffening, and blood pressure can be monitored, and may be able to be used for optimizing countermeasures or detecting emerging cardiovascular emergencies. In order to fully prove the instrument's effectiveness, future work is still needed, but due to practical limitations, this was considered to be beyond the scope of this dissertation. Instead, the focus was on conducting an initial study in short-duration microgravity, and conquering necessary engineering obstacles.

The most challenging engineering obstacle faced was obtaining a high-SNR fixed-platform BCG signal in microgravity. This is because multiple in-band noise sources were present, such as vibration from the vehicle and movement from the subjects. A three-pronged approach of mechanical, analog, and digital filtering methods was paramount in mitigating this. With these methods in place, along with the other methods described in this dissertation, the instrument accomplishes the goals set forth in Section 1.2:

1. Methods were devised for enabling robust measurement of BCG across a population of subjects in the confined microgravity environment of parabolic flight.

2. The quality of the signals obtained with respect to the alternative state of the art was quantified.

3. A number of features in the BCG combined with ECG and PPG were validated to be able to detect parameter changes relevant to cardiovascular deconditioning.

6.2 Future Directions

Out of the future work suggested in Chapters 3–5, the next most effective engineering step would be to redesign the fixed-platform BCG sensor to use a high-bandwidth force plate sensor. This would increase measurement accuracy, avoid the amplitude calibration problem mentioned in Section 3.5.4, and measure on three axes instead of one, resulting in an overall more capable instrument. The next most effective experimental step would be to use a supine reference position in normal gravity in order to better match the fluid position in the body between microgravity and normal gravity. This would enable more clear results about microgravity-induced physiological changes without the complication of also measuring the fluid shift. With these next steps completed, longer duration experiments (e.g., aboard ISS) should then be conducted in order to measure hemodynamic changes induced by longer exposure to microgravity, rather than the transient changes induced by parabolic flight.

6.3 Final Remarks

The technology developed and discussed in this dissertation could significantly increase the ability to study and actively monitor dangerous cardiovascular change in microgravity by providing a new measurement platform. The growing importance of space flight and the lack of a solution define the main motivation of this research: finding a practical solution for hemodynamic monitoring in microgravity. The hope is that the methods devised in this work can be used by astronauts and increase their ability to maintain good health aboard spacecrafts and post flight.

Bibliography

[1] R. L. Hughson, A. Helm, and M. Durante, "Heart in space: Effect of the extraterrestrial environment on the cardiovascular system," *Nature Reviews Cardiology*, vol. 15, 2018.

[2] "NASA strategic plan 2018," National Aeronautics and Space Administration, Tech. Rep., 2018.

[3] "Federal space program 2016-2025," Roscosmos State Corporation for Space Activities, Tech. Rep., 2015.

[4] A. Bowe, "China's pursuit of space power status and implications for the United States," U.S.-China Economic and Security Review Commission, Tech. Rep., 2019.

[5] H. Oberth, *Wege zur Raumschiffahrt*, 3rd ed. De Gruyter, 1929.

[6] C. R. Doarn, V. A. Lavrentyev, O. I. Orlov, A. E. Nicogossian, A. I. Grigoriev, E. W. Ferguson, and R. C. Merrell, "Evolution of telemedicine in Russia: The influence of the space program on modern telemedicine programs," *Telemedicine Journal and e-Health*, vol. 9, no. 1, 2003.

[7] S. M. Abdullah, J. L. Hastings, S. Shibata, S. H. Platts, D. R. Hamilton, J. D. Thomas, D. E. Hughes, M. W. Bungo, and B. D. Levine, "Abstract 18672: Effects of prolonged space flight on cardiac structure and function," *Circulation*, vol. 128, 2018.

[8] A. D. Moore, M. E. Downs, S. M. C. Lee, A. H. Feiveson, P. Knudsen, and L. Ploutz-Snyder, "Peak exercise oxygen uptake during and following long-duration spaceflight," *Journal of Applied Physiology*, vol. 117, 2014.

[9] D. E. Watenpaugh, "The cardiovascular system in microgravity," in *Handbook of Physiology: Environmental Physiology*, M. Fregly and C. Blatteis, Eds. Oxford University Press, 1996, ch. 29.

[10] R. Videbaek and P. Norsk, "Atrial distension in humans during microgravity induced by parabolic flights," *Journal of Applied Physiology*, vol. 83, no. 6, 1997.

[11] M. Estenne, M. Gorini, A. V. Muylem, V. Ninane, and M. Paiva, "Rib cage shape and motion in microgravity," *Journal of Applied Physiology*, vol. 73, 1992.

[12] *Sources and effects of ionizing radiation report (2008).* New York: United Nations Scientific Committee on the Effects of Atomic Radiation, 2010, no. ISBN 978-92-1-142274-0.

[13] *Report No. 160, Ionizing radiation exposure of the population of the United States.* Bethesda, MD: National Council on Radiation Protection and Measurement, 2009, no. ISBN 978-0-929600-98-7.

[14] C. Zeitlin, D. M. Hassler, F. A. Cucinotta, B. Ehresmann, R. F. Wimmer-Schweingruber, D. E. Brinza, S. Kang, G. Weigle, S. Böttcher, E. Böhm, S. Burmeister, J. Guo, J. Köhler, C. Martin, A. Posner, S. Rafkin, and G. Reitz, "Measurements of energetic particle radiation in transit to Mars on the Mars science laboratory," *Science*, vol. 340, no. 6136, 2013.

[15] F. A. Cucinotta and M. Durante, "Cancer risk from exposure to galactic cosmic rays: Implications for space exploration by human beings," *Lancet Oncology*, vol. 7, no. 5, 2006.

[16] M. Durante and F. A. Cucinotta, "Physical basis of radiation protection in space travel," *Reviews of Modern Physics*, vol. 83, no. 4, 2011.

[17] T. C. Slaba, A. A. Bahadori, B. D. Reddell, R. C. Singleterry, M. S. Clowdsley, and S. R. Blattnig, "Optimal shielding thickness for galactic cosmic ray environments," *Life Sciences in Space Research*, vol. 12, 2017.

[18] M. P. Little, E. J. Tawn, I. Tzoulaki, R. Wakeford, G. Hildebrandt, F. Paris, S. Tapio, and P. Elliot, "Review and meta-analysis of epidemiological associations between low/moderate doses of ionizing radiation and circulatory disease risks, and their possible mechanisms," *Radiation and Environmental Biophysics*, vol. 23, no. 1, 2005.

[19] B. Baselet, C. Rombouts, A. M. Benotmane, S. Baatout, and A. Aerts, "Cardiovascular diseases related to ionizing radiation: The risk of low-dose exposure (review)," *International Journal of Molecular Medicine*, vol. 38, no. 6, 2016.

[20] P. Norsk, "Adaptation of the cardiovascular system to weightlessness: Surprises, paradoxes and implications for deep space missions," *Acta physiologica*, vol. 228, no. 3, 2020.

[21] J. V. Meck, C. J. Reyes, S. A. Perez, A. L. Goldberger, and M. G. Ziegler, "Marked exacerbation of orthostatic intolerance after long- vs. short-duration spaceflight in veteran astronauts," *Psychosomatic Medicine*, vol. 63, no. 6, 2001.

[22] C. P. Alfrey, M. M. Udden, C. Leach-Huntoon, T. Driscoll, and M. H. Pickett, "Control of red blood cell mass in spaceflight," *Journal of Applied Physiology*, vol. 81, no. 1, 1996.

[23] P. Norsk, "Vasorelaxation in space," *Hypertension*, vol. 47, no. 1, 2006.

[24] A. Ertl, A. Diedrich, I. Biaggioni, B. Levine, R. Robertson, J. Cox, J. Zuckerman, J. Pawelczyk, C. Ray, J. Buckey Jr., L. Lane, R. Shiavi, F. Gaffney, F. Costa, C. Holt, C. Blomqvist, D. Eckberg, F. Baisch, and D. Robertson, "Human muscle sympathetic nerve activity and plasma noradrenaline kinetics in space," *Journal of Physiology*, vol. 538, 2002.

[25] R. L. Johnson, G. W. Hoffler, A. E. Nicogossian, and S. A. Bergman Jr., "Skylab experiment M-092: Results of the first manned mission," *Acta Astronautica*, vol. 2, no. 3-4, 1975.

[26] P. Norsk and N. J. Christensen, "The paradox of systemic vasodilatation and sympathetic nervous stimulation in space," *Respiratory Physiology & Neurobiology*, vol. 169, 2009.

[27] R. L. Hughson, A. D. Robertson, P. Arbeille, J. K. Shoemaker, J. W. E. Rush, K. S. Fraser, and D. K. Greaves, "Increased postflight carotid artery stiffness and inflight insulin resistance resulting from 6-mo spaceflight in male and female astronauts," *American Journal of Physiology-Heart and Circulatory Physiology*, vol. 310, 2016.

[28] E. C. Tuday, J. V. Meck, D. Nyhan, A. A. Shoukas, and D. E. Berkowitz, "Microgravity-induced changes in aortic stiffness and their role in orthostatic intolerance," *Journal of Applied Physiology*, 2007.

[29] P. Arbeille, R. Provost, and K. Zuj, "Carotid and femoral artery intima-media thickness during 6 months of spaceflight," *Aerospace Medicine and Human Performance*, vol. 87, no. 5, 2016.

[30] G. F. Mitchell, "Arterial stiffness: Insights from Framingham and Iceland," *Current Opinion in Nephrology and Hypertension*, vol. 24, 2015.

[31] S. Greenwald, "Ageing of the conduit arteries," *Journal of Pathology*, vol. 211, 2007.

[32] G. F. Mitchell, H. Parise, E. J. Benjamin, M. G. Larson, M. J. Keyes, J. A. Vita, R. S. Vasan, and D. Levy, "Changes in arterial stiffness and wave reflection with advancing age in healthy men and women. The Framingham Heart Study," *Hypertension*, vol. 43, no. 6, 2004.

[33] G. F. Mitchell, M. A. Van Buchem, S. Sigurdsson, J. D. Gotal, M. K. Jonsdottir, O. lafur Kjartansson, M. Garcia, T. Aspelund, T. B. Harris, V. Gudnason,

and L. J. Launer, "Arterial stiffness, pressure and flow pulsatility and brain structure and function: The age, gene/environment susceptibility – Reykjavik Study," *Brain*, vol. 134, 2011.

[34] W. W. Nichols and D. G. Edwards, "Arterial elastance and wave reflection augmentation of systolic blood pressure: Deleterious effects and implications for therapy," *Journal of Cardiovascular Pharmacology and Therapeutics*, vol. 6, no. 1, 2001.

[35] S. Cheng and R. S. Vasan, "Advances in the epidemiology of heart failure and left ventricular remodeling," *Circulation*, vol. 124, no. 20, 2011.

[36] B. L. Langille, "Remodeling of developing and mature arteries: Endothelium, smooth muscle, and matrix," *Journal of Cardiovascular Pharmacology*, vol. 21, no. Suppl 1:S11-7, 1993.

[37] C. S. Leach, P. C. Johnson, and N. Cintrón, "The endocrine system in space flight," *Acta Astronautica*, vol. 17, no. 2, 1988.

[38] S. J. Zieman, V. Melenovsky, and D. A. Kass, "Mechanisms, pathophysiology, and therapy of arterial stiffness," *Arteriosclerosis, Thrombosis, and Vascular Biology*, vol. 25, no. 5, 2005.

[39] T. J. LaRocca, C. R. Martens, and D. R. Seals, "Nutrition and other lifestyle influences on arterial aging," *Ageing Research Reviews*, vol. 39, 2017.

[40] D. R. Seals, "Edward F. Adolph distinguished lecture: The remarkable anti-aging effects of aerobic exercise on systemic arteries," *Journal of Applied Physiology*, vol. 117, no. 5, 2014.

[41] P. Arbeille, R. Provost, N. Vincent, and A. Aubert, "Adaptation of the main peripheral artery and vein to long term confinement (MARS 500)," vol. 9, no. 1, 2014.

[42] R. Ross, S. N. Blair, R. Arena, T. S. Church, J.-P. Despres, B. A. Franklin, W. L. Haskell, L. A. Kaminsky, B. D. Levine, C. J. Lavie, J. Myers, J. Niebauer,

R. Sallis, S. S. Sawada, X. Sui, and U. Wisloff, "Importance of assessing cardiorespiratory fitness in clinical practice: A case for fitness as a clinical vital sign: A scientific statement from the American Heart Association," *Circulation*, vol. 134, no. 24, 2016.

[43] T. Trappe, S. Trappe, G. Lee, J. Widrick, R. Fitts, and D. Costill, "Cardiorespiratory responses to physical work during and following 17 days of bed rest and spaceflight," *Journal of Applied Physiology*, vol. 100, no. 3, 2006.

[44] B. D. Levine, L. D. Lane, D. E. Watenpaugh, F. A. Gaffney, J. C. Buckey, and C. G. Blomqvist, "Maximal exercise performance after adaptation to microgravity," *Journal of Applied Physiology*, vol. 81, no. 2, 1996.

[45] R. H. Fitts, S. W. Trappe, D. L. Costill, P. M. Gallagher, A. C. Creer, P. A. Colloton, J. R. Peters, J. G. Romatowski, J. L. Bain, and D. A. Riley, "Prolonged space flight-induced alterations in the structure and function of human skeletal muscle fibres," *The Journal of Physiology*, vol. 588, no. 18, 2010.

[46] M. A. Perhonen, F. Franco, L. D. Lane, J. C. Buckey, C. G. Blomqvist, J. E. Zerwekh, R. M. Peshock, P. T. Weatherall, and B. D. Levine, "Cardiac atrophy after bed rest and spaceflight," *Journal of Applied Physiology*, vol. 91, no. 2, 2001.

[47] C. Gallo, L. Ridolfi, and S. Scarsoglio, "Cardiovascular deconditioning during long-term spaceflight through multiscale modeling," *Nature Partner Journals Microgravity*, vol. 6, no. 27, 2020.

[48] A. N. Nowbar, M. Gitto, J. P. Howard, D. P. Francis, and R. Al-Lamee, "Mortality from ischemic heart disease," *Circulation: Cardiovascular Quality and Outcomes*, vol. 12, no. 6, 2019.

[49] M. W. Lorenz, H. S. Markus, M. L. Bots, M. Rosvall, and M. Sitzer, "Prediction of clinical cardiovascular events with carotid intima-media thickness: A systematic review and meta-analysis," *Circulation*, vol. 115, no. 4, 2007.

[50] S. C. Darby, M. Ewertz, P. McGale, A. M. Bennet, U. Blom-Goldman, D. Brønnum, C. Correa, D. Cutter, G. Gagliardi, B. Gigante, M.-B. Jensen, A. Nisbet, R. Peto, K. Rahimi, C. Taylor, and P. Hall, "Risk of ischemic heart disease in women after radiotherapy for breast cancer," *The New England Journal of Medicine*, vol. 368, no. 11, 2013.

[51] T. Yu, B. W. Parks, S. Yu, R. Srivastava, K. Gupta, X. Wu, S. Khaled, P. Y. Chang, J. H. Kabarowski, and D. F. Kucik, "Iron-ion radiation accelerates atherosclerosis in apolipoprotein E-deficient mice," *Radiation Research*, vol. 175, no. 6, 2011.

[52] Y. Takahashi, T. Teshima, N. Kawaguchi, Y. Hamada, S. Mori, A. Madachi, S. Ikeda, H. Mizuno, T. Ogata, K. Nojima, Y. Furusawa, and N. Matsuura, "Heavy ion irradiation inhibits in vitro angiogenesis even at sublethal dose," *Cancer Research*, vol. 63, no. 14, 2003.

[53] M. Tungjai, E. B. Whorton, and K. N. Rithidech, "Persistence of apoptosis and inflammatory responses in the heart and bone marrow of mice following whole-body exposure to ^{28}Silicon (^{28}Si) ions," *Radiation and Environmental Biophysics*, vol. 52, no. 3, 2013.

[54] M. D. Delp, J. M. Charvat, C. L. Limoli, R. K. Globus, and P. Ghosh, "Apollo lunar astronauts show higher cardiovascular disease mortality: Possible deep space radiation effects on the vascular endothelium," *Scientific Reports*, vol. 6, no. 29901, 2016.

[55] F. A. Cucinotta, N. Hamada, and M. P. Little, "No evidence for an increase in circulatory disease mortality in astronauts following space radiation exposures," *Life Sciences in Space Research*, vol. 10, 2016.

[56] A. R. Hargens, R. Bhattacharya, and S. M. Schneider, "Space physiology VI: Exercise, artificial gravity,and countermeasure development for prolonged space flight," *European Journal of Applied Physiology*, vol. 113, 2013.

[57] S. Iwase, H. Takada, Y. Watanabe, K. Ishida, H. Akima, K. Katayama, M. Iwase, K. Hirayanagi, T. Shiozawa, T. Hamaoka, Y. Masuo, and M.-A. Custaud, "Effect of centrifuge-induced artificial gravity and ergometric exercise on cardiovascular deconditioning, myatrophy, and osteoporosis induced by a -6 degrees head-down bedrest," *Journal of Gravitational Physiology*, vol. 11, no. 2, 2004.

[58] S. Iwase, "Effectiveness of centrifuge-induced artificial gravity with ergometric exercise as a countermeasure during simulated microgravity exposure in humans," *Acta Astronautica*, vol. 57, no. 2-8, 2005.

[59] V. J. Caiozzo, F. Haddad, S. Lee, M. Baker, W. Paloski, and K. M. Baldwin, "Artificial gravity as a countermeasure to microgravity: A pilot study examining the effects on knee extensor and plantar flexor muscle groups," *Journal of Applied Physiology*, vol. 107, no. 1, 2009.

[60] M. B. Stenger, J. M. Evans, C. F. Knapp, S. M. Lee, T. R. Phillips, S. A. Perez, A. D. Moore Jr., W. H. Paloski, and S. H. Platts, "Artificial gravity training reduces bed rest-induced cardiovascular deconditioning," *European Journal of Applied Physiology*, vol. 112, no. 2, 2012.

[61] A. R. Hargens, B. R. Macias, C. M. Echon, E. Brzezinski, A. Hawkins, K. Hawkins, and R. S. Meyer, "Testing exercise countermeasures during 30 days of simulated microgravity: Lessons learned from studies of identical twins," *Gravitational and Space Research*, vol. 19, no. 2, 2006.

[62] M. W. Bungo, J. B. Charles, and P. C. Johnson Jr., "Cardiovascular deconditioning during space flight and the use of saline as a countermeasure to orthostatic intolerance," *Aviation, Space, and Environmental Medicine*, vol. 56, no. 10, 1985.

[63] M. Durante, "Space radiation protection: Destination Mars," *Life Sciences in Space Research*, vol. 1, 2014.

[64] M. Balasingam, J. Ebrahimb, and I. Ariffinb, "Tele-echocardiography – made for astronauts, now in hospitals," *Indian Heart Journal*, vol. 69, 2017.

[65] R. Mukkamala, J.-O. Hahn, O. T. Inan, L. K. Mestha, C.-S. Kim, H. Toreyin, and S. Kyal, "Toward ubiquitous blood pressure monitoring via pulse transit time: Theory and practice," *IEEE Transactions on Biomedical Engineering*, vol. 62, no. 8, 2015.

[66] K. H. Wesseling, J. R. Jansen, J. J. Settels, and J. Schreuder, "Computation of aortic flow from pressure in humans using a nonlinear, three-element model," *Journal of Applied Physiology*, vol. 74, 1993.

[67] M. P. Harms, K. H. Wesseling, F. Pott, M. Jenstrup, J. Van Goudoever, N. H. Secher, and J. J. Van Lieshout, "Continuous stroke volume monitoring by modelling fow from non-invasive measurement of arterial pressure in humans under orthostatic stress." *Clinical Science*, vol. 97, 1999.

[68] J. Villa, T. Shaw, W. Toscano, and P. Cowings, "Evaluation of astroskin biomonitor during high intensity physical activities," *Memorias Del Congreso Nacional De Ingenieria Biomedica*, vol. 5, no. 1, 2018.

[69] G. K. Prisk, S. Verhaeghe, D. Padeken, H. Hamacher, and M. Paiva, "Three-dimensional ballistocardiography and respiratory motion in sustained microgravity," *Aviation Space and Environmental Medicine*, vol. 72, no. 12, 2001.

[70] P.-F. Migeotte, S. D. Ridder, J. Tank, N. Pattyn, I. Funtova, R. Baevsky, X. Neyt, and G. K. Prisk, "Three dimensional ballisto- and seismocardiography: HIJ wave amplitudes are poorly correlated to maximal systolic force vector," in *Proceedings of the 2012 Annual International Conference of the IEEE Engineering in Medicine and Biology Society*, San Diego, CA, 2012.

[71] I. Starr, A. J. Rawson, H. A. Schroeder, and N. R. Joseph, "Studies on the estimation of cardiac output in man, and of abnormalities in cardiac function from the heart's recoil and the blood's impact; the ballistocardiogram," *American Journal of Physiology*, vol. 127, no. 1, 1939.

[72] O. T. Inan, M. Etemadi, A. Paloma, L. Giovangrandi, and G. T. A. Kovacs, "Non-invasive cardiac output trending during exercise recovery on a bathroom-scale-based ballistocardiograph," *Physiological Measurement*, vol. 30, no. 3, 2009.

[73] M. Etemadi, O. T. Inan, L. Giovangrandi, and G. T. A. Kovacs, "Rapid assessment of cardiac contractility on a home bathroom scale," *IEEE Transactions on Information Technology in Biomedicine*, vol. 15, no. 6, 2011.

[74] J. H. Shin, K. M. Lee, and K. S. Park, "Non-constrained monitoring of systolic blood pressure on a weighing scale," *Physiological Measurement*, vol. 30, no. 7, 2009.

[75] R. Casanella, J. Gomez-Clapers, and R. Pallas-Areny, "On time interval measurements using BCG," in *Proceedings of the 2012 Annual International Conference of the IEEE Engineering in Medicine and Biology Society*, San Diego, CA, 2012.

[76] Q. Deliere, P.-F. Migeotte, X. Neyt, I. Funtova, R. Baevsky, J. Tank, and N. Pattyn, "Cardiovascular changes in parabolic flights assessed by ballistocardiography," in *Proceedings of the 2013 Annual International Conference of the IEEE Engineering in Medicine and Biology Society*, Osaka, Japan, 2013.

[77] O. T. Inan, M. Etemadi, R. M. Wiard, G. T. A. Kovacs, and L. Giovangrandi, "Non-invasive measurement of valsalva-induced hemodynamic changes on a bathroom scale ballistocardiograph," in *Proceedings of the 2008 Annual International Conference of the IEEE Engineering in Medicine and Biology Society*, Vancouver, B.C., 2008.

[78] J. W. Gordon, "On certain molar movements of the human body produced by the circulation of the blood," *Journal of Anatomy and Physiology*, vol. 11, 1877.

[79] L. Giovangrandi, O. T. Inan, R. M. Wiard, M. Etemadi, and G. T. A. Kovacs, "Ballistocardiography – a method worth revisiting," in *Proceedings of the*

2011 Annual International Conference of the IEEE Engineering in Medicine and Biology Society, Boston, Massachusetts, 2011.

[80] C.-S. Kim, S. L. Ober, M. S. McMurtry, B. A. Finegan, O. T. Inan, R. Mukkamala, and J.-O. Hahn, "Ballistocardiogram: Mechanism and potential for unobtrusive cardiovascular health monitoring," *Scientific Reports*, vol. 6, no. 1, 2016.

[81] O. T. Inan, M. Etemadi, R. M. Wiard, L. Giovangrandi, and G. T. A. Kovacs, "Robust ballistocardiogram acquisition for home monitoring," *Physiological Measurement*, vol. 30, 2009.

[82] J. Gomez-Clapers, A. Serra-Rocamora, R. Casanella, and R. Pallas-Areny, "Uncertainty factors in time-interval measurements in ballistocardiography," in *Proceedings of the 19th IMEKO TC-4 Symposium and 17th IWADC Workshop: Advances in Instrumentation and Sensors Interoperability*, Barcelona, Spain, 2013.

[83] O. T. Inan, M. Etemadi, B. Widrow, and G. T. A. Kovacs, "Adaptive cancellation of floor vibrations in standing ballistocardiogram measurements using a seismic sensor as a noise reference," *IEEE Transactions on Biomedical Engineering*, vol. 57, no. 3, 2010.

[84] O. T. Inan, G. T. A. Kovacs, and L. Giovangrandi, "Evaluating the lower-body electromyogram signal acquired from the feet as a noise reference for standing ballistocardiogram measurements," *IEEE Transactions on Information Technology in Biomedicine*, vol. 14, no. 5, 2010.

[85] J. Blacher, R. Asmar, S. Djane, G. M. London, and M. E. Safar, "Aortic pulse wave velocity as a marker of cardiovascular risk in hypertensive patients," *Hypertension*, vol. 33, no. 5, 1999.

[86] J. Erlanger and D. R. Hooker, *An experimental study of blood-pressure and of pulse-pressure in man.* from the Physiological Laboratory of the Johns Hopkins University, 2011.

[87] R. P. Lewis, S. E. Rittgers, W. F. Forester, and H. Boudoulas, "A critical review of the systolic time intervals," *Circulation*, vol. 56, no. 2, 1977.

[88] Y. G. Lim, K. H. Hong, K. K. Kim, J. H. Shin, and K. S. Park, "Mechanocardiogram measured at the back of subjects sitting in a chair as a non-intrusive pre-ejection period measurement," in *Proceedings of the 2006 Pervasive Health Conference and Workshops*, Innsbruck, Austria, 2006.

[89] D. D. He, E. S. Winokur, and C. G. Sodini, "A continuous, wearable, and wireless heart monitor using head ballistocardiogram (BCG) and head electrocardiogram (ECG)," in *Proceedings of the 2011 Annual International Conference of the IEEE Engineering in Medicine and Biology Society*, Boston, Massachusetts, 2011.

[90] W. W. Nichols, M. F. O'Rourke, and C. Vlachopoulos, *McDonald's blood flow in arteries: Theoretic, experimental, and clinical principles.* Hodder Arnold, 2011.

[91] L. M. Van Bortela, S. Laurentb, P. Boutouyrieb, P. Chowienczykc, J. K. Cruickshankd, T. D. Backera, J. Filipovskye, S. Huybrechtsa, F. U. Mattace-Rasof, A. D. Protogeroug, G. Schillacih, P. Segersi, S. Vermeerscha, and T. Weberj, "Expert consensus document on the measurement of aortic stiffness in daily practice using carotid-femoral pulse wave velocity," *Journal of Hypertension*, vol. 30, no. 3, 2012.

[92] W. Chen, T. Kobayashi, S. Ichikawa, Y. Takeuchi, and T. Togawa, "Continuous estimation of systolic blood pressure using the pulse arrival time and intermittent calibration," *Medical and Biological Engineering and Computing*, vol. 38, 2000.

[93] G. Zhang, M. Gao, D. Xu, N. B. Olivier, and R. Mukkamala, "Pulse arrival time is not an adequate surrogate for pulse transit time as a marker of blood pressure," *Journal of Applied Physiology*, vol. 111, no. 6, 2011.

[94] S. L.-O. Martin, A. M. Carek, C.-S. Kim, H. Ashouri, O. T. Inan, J.-O. Hahn, and R. Mukkamala, "Weighing scale-based pulse transit time is a superior marker of blood pressure than conventional pulse arrival time," *Scientific Reports*, vol. 6, 2016.

[95] J. Gomez-Clapers, R. Casanella, and R. Pallas-Areny, "Direct pulse transit time measurement from an electronic weighing scale," in *Proceedings of the 2016 IEEE Computing in Cardiology Conference*, Vancouver, B.C., 2016.

[96] National Aeronautics and Space Administration. (2022) Orion by the numbers. [Online]. Available: https://www.nasa.gov/sites/default/files/fs-2014-08-004-jsc-orion_quickfacts-web.pdf

[97] D. Smitherman, T. Russell, M. Baysinger, P. Capizzo, L. Fabisinski, B. Griffin, L. Hornsby, D. Maples, and J. Miernik, "Deep space habitat configurations based on international space station systems," NASA Advanced Concepts Office, Tech. Rep., 2011.

[98] M. Rudisill, R. Howard, B. Griffin, J. Green, L. Toups, and K. Kennedy, "Lunar architecture team - phase 2 habitat volume estimation: Caution when using analogs," National Aeronautics and Space Administration, Tech. Rep., 2008.

[99] Business Air News. Boeing B-727 — Handbook. [Online]. Available: https://www.businessairnews.com/hb_aircraftpage.html?recnum=B727

[100] B. Pump, R. Videaek, A. Gabrielsen, and P. Norsk, "Arterial pressure in humans during weightlessness induced by parabolic flights," *Journal of Applied Physiology*, vol. 87, no. 3, 1999.

[101] L. G. Petersen, M. Damgaard, J. C. Petersen, and P. Norsk, "Mechanisms of increase in cardiac output during acute weightlessness in humans," *Journal of Applied Physiology*, vol. 111, no. 2, 2011.

[102] T. P. Moore and W. E. Thornton, "Space shuttle inflight and postflight fluid shifts measured by leg volume changes," *Aviation, Space, and Environmental Medicine*, vol. 59, no. 9, 1987.

[103] K. Marshall-Goebel, S. S. Laurie, I. V. Alferova, P. Arbeille, S. M. Aunon-Chancellor, D. J. Ebert, S. M. Lee, B. R. Macias, D. S. Martin, J. M. Pattarini, R. Ploutz-Snyder, L. C. Ribeiro, W. J. Tarver, S. A. Dulchavsky, A. R. Hargens, and M. B. Stenger, "Assessment of jugular venous blood flow stasis and thrombosis during spaceflight," *JAMA Network Open*, vol. 2, no. 11, 2019.

[104] R. L. Hughson, J. K. Shoemaker, A. P. Blaber, P. Arbeille, D. K. Greaves, P. P. Pereira-Junior, and D. Xu, "Cardiovascular regulation during long-duration spaceflights to the International Space Station," *Journal of Applied Physiology*, vol. 112, no. 5, 2012.

[105] B. E. Shykoff, L. E. Farhi, A. J. Olszowka, D. R. Pendergast, M. A. Rokitka, C. G. Eisenhardt, and R. A. Morin, "Cardiovascular response to submaximal exercise in sustained microgravity," *Journal of Applied Physiology*, vol. 81, no. 1, 1996.

[106] M. K. Wilkerson, J. Muller-Delp, P. N. Colleran, and M. D. Delp, "Effects of hindlimb unloading on rat cerebral, splenic, and mesenteric resistance artery morphology," *Journal of Applied Physiology*, vol. 87, no. 6, 1999.

[107] M. B. Rappaport, H. B. Sprague, and W. B. Thompson, "Ballistocardiography I. physical considerations," *Circulation*, vol. 7, no. 2, 1953.

[108] J. Alametsa, A. Varri, M. Koivuluoma, and L. Barna, "The potential of EMFi sensors in heart activity monitoring," in *Proceedings of the 2nd Open ECG Workshop Integration of the ECG into the HER & Interoperability of ECG Device Systems*, Berlin, Germany, 2004.

[109] A. Savitzky and M. J. Golay, "Soothing and differentiation of data by simplified least squares procedures," *Analytical Chemistry*, vol. 36, 1964.

[110] O. T. Inan, L. Giovangrandi, and G. T. A. Kovacs, "Robust neural-network-based classification of premature ventricular contractions using wavelet transform and timing interval features," *IEEE Transactions of Biomedical Engineering*, vol. 53, no. 12, 2006.

[111] N. J. Bershad and A. J. Rockmore, "On estimating signal-to-noise ratio using the sample correlation coefficient," *IEEE Transactions of Information Theory*, vol. 20, no. 1, 1974.

[112] O. T. Inan, P.-F. Migeotte, K.-S. Park, M. Etemadi, K. Tavakolian, R. Casanella, J. Zanetti, J. Tank, I. Funtova, G. K. Prisk, and M. D. Rienzo, "Ballistocardiography and seismocardiography: A review of recent advances," *IEEE Journal of Biomedical and Health Informatics*, vol. 19, no. 4, 2015.

[113] H. Ashouri, L. Orlandic, and O. T. Inan, "Unobtrusive estimation of cardiac contractility and stroke volume changes using ballistocardiogram measurements on a high bandwidth force plate," *IEEE Transactions of Information Theory*, vol. 16, no. 6, 2016.

[114] R. M. Wiard, O. T. Inan, L. Giovangrandi, C. M. Cuttino, and G. T. A. Kovacs, "Preliminary results from standing ballistocardiography measurements in microgravity," in *Proceedings of the 2013 Annual International Conference of the IEEE Engineering in Medicine and Biology Society*, Osaka, Japan, 2013.

[115] C. McCall, Z. Stuart, R. M. Wiard, O. T. Inan, L. Giovangrandi, C. M. Cuttino, and G. T. A. Kovacs, "Standing ballistocardiography measurements in microgravity," in *Proceedings of the 2014 Annual International Conference of the IEEE Engineering in Medicine and Biology Society*, Chicago, IL, 2014.

[116] C. McCall, R. Rostosky, R. M. Wiard, O. T. Inan, L. Giovangrandi, C. M. Cuttino, and G. T. A. Kovacs, "Noninvasive pulse transit time measurement for arterial stiffness monitoring in microgravity," in *Proceedings of the 2015 Annual International Conference of the IEEE Engineering in Medicine and Biology Society*, Milan, Italy, 2015.

[117] K. Ikedal, A. Iwamura, M. Shioikari, H. Kashihara, O. Miura, M. Morooka, A. Kojima, M. Seko, K. Nakamura, H. Ohkawa, T. Tanaka, H. Sugiyama, H. Yokota, Y. Iwasaki, A. Kuwajima, and M. Tamura, "Serial measurement of brachial-ankle administration pulse wave velocity after intramuscularly of

scopolamine butylbromide," *Health Evaluation and Promotion*, vol. 30, no. 4, 2003.